An automatically well-balanced formulation of pressure forcing for discontinuous Galerkin methods for the shallow water equations

Robert L. Higdon

Department of Mathematics, Oregon State University, Corvallis, Oregon 97331-4605, United States

ARTICLE INFO

ABSTRACT

This paper begins a development of methods for addressing variable bottom topography in discontinuous Galerkin numerical methods for multi-layer, variable-density models of ocean circulation. For numerical models of ocean circulation, it is a widespread practice to split the fast (external) and slow (internal) dynamics into separate subsystems that are solved by different techniques. The fast dynamics are modeled by a vertically-integrated system that is very similar to the shallow water equations for a hydrostatic fluid of constant density. As a first step, the present paper focuses on variable bottom topography for the shallow water equations; extensions to the multi-layer case will be reported elsewhere.

A central point of this work, for both the shallow water and the multi-layer cases, is the representation of the pressure forcing in the momentum equations. For the shallow water case, the present work does not use the standard representation of the pressure forcing that is widely used for the shallow water system. Instead, it begins with a more basic form of the momentum equations for a fluid flow, and it proceeds directly to a weak Galerkin form via integration over a suitable fluid region. The resulting formulation of the momentum equations is automatically well-balanced, subject to an assumption that the algorithms used to compute quantities at cell edges reproduce the continuous values in the case where all functions involved are continuous. In addition, this formulation has a structure that is analogous to that of the momentum equations in the individual layers of a multi-layer fluid, and this facilitates consistency between the two subsystems that are used to model such a fluid.

The numerical computations described here include tests of well-balancing and tests of wave propagation over variable topography.

1. Introduction

This paper is part of a continuing effort to develop, analyze, and test various procedures for using discontinuous Galerkin (DG) numerical methods for multi-layer models of ocean circulation. Some previous work by this author on this topic is described in [7], [8], and [9]. The present paper describes the first part of additional work that addresses the problem of variable topography at the bottom of the fluid region.

A summary of the previous work is the following. The first paper [7] develops weak Galerkin forms for the mass and momentum equations in the case of a general vertical coordinate (e.g., z, density, terrain-fitted, or a hybrid coordinate), with particular attention paid to the lateral pressure forcing in the momentum equations. The paper then restricts attention to the shallow water equations for a hydrostatic fluid of constant density, and for that case it analyzes numerical dispersion relations and time-stepping methods. The second paper [8] addresses multi-layer modeling of a variable-density stratified fluid, with density as a vertical coordinate. A focus of this paper is barotropic-baroclinic time splitting for handling the multiple time scales that are found in this situation. The numerical computations described in that paper demonstrate accurate simulation of geostrophic adjustment, an important mechanism in the time evolution of large-scale oceanic flows. The third paper [9] develops a representation of horizontal viscosity in the momentum equations, in a way that can be used with a DG spatial discretization and a barotropic-baroclinic time splitting. The paper also develops a limiter that maintains nonnegative numerical values of layer thicknesses in situations where the dynamics of the flow can generate thin fluid layers, such as during upwelling events.

These preceding papers paid little attention to interactions with variable bottom topography, and in almost all of the numerical computations the bottom of the fluid region was assumed to be flat and level. The present paper begins a study of variable bottom topography, and it focuses on the case of the constant-density shallow water equations. In a barotropic-baroclinic splitting for a variable-density multi-layer fluid, the fast motions are represented by a vertically-integrated, lower-dimensional ("barotropic") system that is similar to the shallow water equations. The present discussion of variable topography for the shallow water system is thus one step towards the goal of handling bottom topography in multi-layer models. Extensions of this work to multi-layer fluids will be addressed elsewhere. The shallow water equations are also of independent interest in their own right, due to their role in modeling processes such as tides (Pringle et al., [14]), storm surges (Dawson et al. [4]), and tsunamis (Bonev et al. [3], LeVeque et al. [11]).

The present work for the shallow water equations is based on ideas for variable-density stratified flows that are included in the first paper [7]. For the case of a general vertical coordinate as analyzed in [7], surfaces of constant vertical coordinate need not be horizontal. However, the lateral pressure forcing must act in a direction that is truly horizontal, regardless of the choice of vertical coordinate. This fact causes

e-mail: Robert.Higdon@oregonstate.edu (Robert L. Higdon)

some difficulties if one wants to produce a pointwise partial differential equation, in terms of the given vertical coordinate, and then produce a DG discretization. However, with a DG method one does not really need a pointwise partial differential equation; instead, all that one really needs is an integral weak form. The approach taken in [7] is to proceed directly to a weak form by multiplying the lateral pressure forcing by a test function, integrating over a suitable fluid region, and then applying a multi-dimensional version of integration by parts.

The present paper employs an analogous maneuver for the case of the constant-density shallow water equations. In this case, the region of integration consists of the entire water column that resides in a grid cell, and the result is a representation of the lateral pressure forcing that is substantially different from the standard representation; the latter is described later in this paper. If the present strategy is used for the barotropic (vertically-integrated) equations for a multi-layer model, then the barotropic equations have a structure that is analogous to that of the equations in the individual layers. This relationship facilitates the consistency between the two subsystems in a barotropic-baroclinic splitting; the issue of consistency is discussed in [8].

The present strategy for pressure forcing has an additional benefit. A well-known issue with variable bottom topography that can arise in the case of the shallow water equations is the problem of well-balancing. In the widely-used formulation of this system, the pressure forcing in the momentum equation generates a time-independent term that involves the gradient of the elevation of the bottom boundary of the fluid region. Unless special care is taken, this term can act as a static forcing term that causes a stationary fluid to start to move, as represented in a numerical simulation, even though the physical circumstances imply that the fluid should remain at rest. In response to this problem, various well-balanced numerical methods have been developed; see, e.g., [3], [11], Liu [13], Xing et al., [16], Yang et al. [17], and the references cited therein.

However, the issues described in the preceding paragraph can be avoided with the representation of pressure forcing that is developed in the present paper. The matter of well-balancing arises ultimately from producing a pointwise system of partial differential equations whose unknowns are the horizontal components of velocity and the thickness of the fluid layer. On the other hand, the method in the present paper skips this step, and instead it proceeds directly from a generic form of the momentum equations to an integral weak form that can be implemented in a DG method. In this case, the pressure forcing is automatically well-balanced, in the sense that no special procedures are needed in order to obtain this property. As with any DG method, it is necessary to compute certain quantities at the edges of grid cells, based on data in the adjacent cells; it is assumed here that the algorithms used to compute pressure values at a cell edge reproduce the continuous values in situations where all of the functions involved are continuous across that edge. In addition, the integrals in the weak form need to be computed with sufficient accuracy. However, nothing beyond these assumptions is needed in order to obtain well-balanced forcing.

The above ideas for the shallow water equations are mentioned briefly in [7]. However, the discussion in

that paper has the following limitations, which are addressed in the present paper.

(1) The earlier paper [7] made only a brief mention of algorithmic issues for the shallow water equations with variable bottom topography, as the paper was focused on other matters. However, subsequent work with the same code with time-dependent problems over variable topography yielded irregular behavior in the computed solutions. This experience necessitated a re-examination of the methods that were being used. This led to a total revision of the process of computing quantities at cell edges, which includes the interpolation of left and right states via Riemann problems.

(2) A proof of well-balancing is included in [7]. However, this proof is unnecessarily restrictive, in that it assumes one particular method for computing quantities at the edges of grid cells. In the present paper, the proof is much more general, and the main idea behind the well-balancing is more apparent.

(3) The derivations in [7] focused on variable-density flows with an arbitrary vertical coordinate. Some results involving the shallow water equations were then obtained by reducing some general results to that special case. However, this manner of development caused the discussion of the shallow water equations to rely entirely on notation that is not standard for that system. The development in the present paper begins with notation that is more standard, so the main ideas are more accessible.

(4) The numerical computations involving variable bottom topography are much more extensive in the present paper.

An outline of this paper is the following. Section 2 states the shallow water equations in terms of the standard representation of the pressure forcing. Section 3 develops the alternate representation and summarizes the development of DG methods for this system. This representation requires vertical integrals of the pressure, both at points in the interiors of grid cells and at the edges of grid cells, and this matter is discussed in Section 4. The calculation at cell edges assumes that a perturbation in bottom pressure (equivalently, free-surface height) has been computed at cell edges, but Section 4 does not assume any particular method for doing this. Instead, this section imposes a modest assumption that the method reproduces the continuous values in the case where all of the functions involved are continuous. Section 5 proves that the pressure forcing is well-balanced, subject to that assumption. Section 6 uses the idea of Riemann problem to produce a method for computing certain quantities at cell edges. Section 7 describes the results of some numerical computations. One set of computations illustrates well-balancing, and the other computations test the ability of the method to model the propagation of traveling waves on regions having variable bottom topography. Section 8 contains a summary.

2. Shallow water equations

This section outlines the two-dimensional shallow water equations for a single-layer fluid, with a focus on the standard representation of the pressure forcing, and it also outlines a motivation for the alternate formulation that is developed in this paper. For the shallow water system, assume that a fluid has constant density and is bounded below by a rigid surface and above by a surface that is free to move. Also assume

that the depth of the fluid is much smaller than the horizontal length scales for the fluid motions of interest; this shallow water assumption implies that the fluid is approximately hydrostatic, i.e., vertical accelerations are negligible (Higdon [6]).

In the horizontal dimensions, use rectangular coordinates x and y, and let z denote the vertical coordinate. Let ρ denote the density of the fluid; $z_{bot}(x, y)$ the elevation of the bottom boundary of the fluid; $z_{top}(x, y, t)$ the elevation of the free surface at the top of the fluid; $h(x, y, t) = z_{top}(x, y, t) - z_{bot}(x, y)$ the thickness of the fluid layer; $u(x, y, z, t)$ and $v(x, y, z, t)$ the x- and y-components of fluid velocity, respectively; f the Coriolis parameter, and $P(x, y, z, t)$ the pressure within the fluid. Assume that the viscosity of the fluid is negligible.

2.1. A standard representation of the pressure forcing.

The shallow water equations are derived by, e.g., Gill [5] and Vallis [15]. The present subsection gives a brief overview of a derivation of this system.

The hydrostatic condition can be expressed as $\partial P / \partial z = -\rho g$. Under the present assumption of constant density, this relation implies

$$P(x, y, z, t) = p_0 + \rho g \big(z_{top}(x, y, t) - z \big), \tag{1}$$

where p_0 is the atmospheric pressure and g is the magnitude of the acceleration due to gravity. In this section, p_0 is assumed to be constant; however, the analysis in Section 3 allows for the possibility of variable p_0. Eq. (1) implies that the horizontal gradient of the pressure P is proportional to the gradient of z_{top}, which is independent of z. If the horizontal components of velocity are initially independent of z, it then follows that they are independent of z for all time, and

$$\frac{\partial u}{\partial t} + u u_x + v u_y - fv = -g \frac{\partial h}{\partial x} - g \frac{\partial z_{bot}}{\partial x} \tag{2}$$

$$\frac{\partial v}{\partial t} + u v_x + v v_y + fu = -g \frac{\partial h}{\partial y} - g \frac{\partial z_{bot}}{\partial y}. \tag{3}$$

The preceding equations use the relation $z_{top}(x, y, t) = h(x, y, t) + z_{bot}(x, y)$ to express the pressure forcing in terms of the unknown h instead of the unknown z_{top}, as h can serve as the mass variable in the present situation. In particular, the conservation of mass can be expressed by the equation

$$\frac{\partial h}{\partial t} + \frac{\partial}{\partial x}(uh) + \frac{\partial}{\partial y}(vh) = 0, \tag{4}$$

since the quantity ρh is the mass per unit horizontal area, and $(u\rho h, v\rho h)$ is the mass flux vector in the horizontal dimensions. The resulting system (2)–(4) consists of three equations with unknowns u, v, and h.

Eqs. (2)–(3) can be regarded as the advective form of the equations for conservation of horizontal momentum. These equations could also be written in momentum-flux form, with dependent variables uh and vh, by multiplying (2)–(3) by h and combining the result with the mass equation (4). The result is

$$\frac{\partial}{\partial t}(uh) + +\frac{\partial}{\partial x}\big(u(uh)\big) + \frac{\partial}{\partial y}\big(v(uh)\big) - fvh = -g\frac{\partial}{\partial x}\left(\frac{1}{2}h^2\right) - gh\frac{\partial z_{bot}}{\partial x} \tag{5}$$

$$\frac{\partial}{\partial t}(vh) + + \frac{\partial}{\partial x}\big(u(vh)\big) + \frac{\partial}{\partial y}\big(v(vh)\big) + fuh \quad = \quad -g\frac{\partial}{\partial y}\left(\frac{1}{2}h^2\right) - gh\frac{\partial z_{bot}}{\partial y} \tag{6}$$

2.2. Some remarks on the standard representation

The momentum equations (2)–(3) contain static terms that involve derivatives of the elevation of the bottom topography. The same is true of the momentum-flux form (5)–(6). Unless sufficient care is taken, numerical discretizations of such terms can generate spurious forcing in the case of variable bottom topography, and this forcing could degrade the quality of numerical solutions. For example, for a fluid that is initially at rest, and with a level free surface, numerical solutions could show nonzero movement, even in the case where no physical forcing is present. In response to this problem, various procedures have been used to obtain "well-balanced" numerical methods for the shallow water equations (e.g., [3], [11], [13], [16], [17]).

The difficulty described here arises from the following. In general, the pressure P depends on (x, y, z, t), but in the present situation the hydrostatic condition enables one to eliminate z from the pressure forcing. Further manipulations yield a pointwise system of partial differential equations with unknowns u, v, and h, which depend on two horizontal dimensions and time. A consequence of this transformation is the presence of the static forcing terms in the case of variable bottom topography.

However, with a discontinuous Galerkin method, one does not really need a pointwise system of partial differential equations; instead, all that one needs is an integral weak form of each of the governing equations. A method for doing this is motivated in Section 2.3 and is developed in detail in Section 3.

2.3. Motivation for the alternate representation

The development in Section 3 is based on the earlier work in [7] for variable-density models that employ a generalized vertical coordinate that includes level, terrain-fitted, isopycnic (density), and hybrid coordinates as special cases. When a generalized coordinate is used, the surfaces of constant vertical coordinate need not be horizontal, but the pressure gradient in the momentum equation needs to be taken in a direction that is truly horizontal. The pressure gradient for a fixed generalized vertical coordinate then requires a correction term to obtain what is really needed. The correct pressure forcing is a sum of two terms, and in some situations these terms could have similar magnitudes but opposite signs. When these individual terms are approximated numerically, their sum could be dominated by error. In addition, the structure of these terms creates complications for a DG implementation.

These problems arise from a desire to produce a pointwise partial differential equation in terms of a given generalized vertical coordinate. However, for a discontinuous Galerkin method, a pointwise equation is not needed. Instead, the technique used in [7] is to go back to the beginning, start over, and produce an integral weak form directly. Begin with the pressure gradient for fixed z (regardless of the generalized vertical coordinate that is used), multiply by a test function, and integrate over a fluid region defined by a grid cell in the horizontal dimensions and a vertical extent determined by two curving surfaces of constant

generalized vertical coordinate. Then integrate by parts. In the special case where the test function is constant, this procedure resembles some methods used by Lin [12] and Adcroft et al. [1] to overcome pressure-gradient errors in finite volume methods.

In the case of a hydrostatic fluid of constant density, the problem with well-balancing described in Section 2.2 arises ultimately from using the hydrostatic condition to eliminate the three-dimensional pressure field and produce a pointwise system with unknowns u, v, and h. Again, a pointwise system is not needed, but instead it suffices to produce an integral weak form. The approach taken in Section 3 is to use the same technique as in [7], except that the region of integration is the entire water column that sits on a grid cell. The result is a formulation that is naturally suited for DG methods, and it has the following advantages.

(1) In the case of a barotropic-baroclinic time splitting for a multi-layer model, the vertically-integrated (fast) barotropic system will then have the same structure as the equations in the layers. It is critical to maintain consistency between the two subsystems [8]; in particular, the vertical sums of the equations in the layers need to coincide with what is used for the barotropic equations, and this is enabled by the technique that is used here.

(2) The pressure forcing is automatically well-balanced, as demonstrated in Section 5 of the present paper.

3. An alternate representation of the pressure forcing

The present section develops the alternate representation of pressure forcing that is mentioned at the end of the preceding section. This section concludes with a summary of the weak forms of the governing equations and a summary of how these weak forms are used to develop a discontinuous Galerkin numerical method.

As in Section 2, consider an inviscid fluid of constant density that satisfies the shallow water (i.e., hydrostatic) assumption. In general, the horizontal momentum equations can be written as

$$\frac{\partial u}{\partial t} + uu_x + vu_y + wu_z - fv = -\frac{1}{\rho}\frac{\partial P}{\partial x} \tag{7}$$

$$\frac{\partial v}{\partial t} + uv_x + vv_y + wv_z + fu = -\frac{1}{\rho}\frac{\partial P}{\partial y}. \tag{8}$$

As before, it will be assumed that the horizontal velocity is initially independent of z at all locations. It follows from the analysis in Section 2.1 that u and v are independent of z at all locations and times, so the quantities u_z and v_z in Eq. (7)–(8) are zero. The preceding conclusion follows from the representation of the three-dimensional pressure P in Eq. (1), but that representation will not be used in the derivation of the weak Galerkin form that is given below, due to the consequences outlined in Section 2.2.

For the sake of simplicity in the following analysis, also assume that all quantities are independent of y; this assumption allows the possibility of nonzero values of the y-component of velocity, so the Coriolis effect

is present. Under this assumption, the equations Eq. (7)–(8) reduce to

$$\frac{\partial u}{\partial t} + uu_x - fv \;=\; -\frac{1}{\rho}\frac{\partial P}{\partial x} \tag{9}$$

$$\frac{\partial v}{\partial t} + uv_x + fu \;=\; 0. \tag{10}$$

The alternate representation of the pressure forcing will be developed in the context of this system.

In the present case, the spatial domain is an interval in x. Partition this interval into grid cells, and let $D_j = [x_{j-1/2}, \; x_{j+1/2}]$ be such a cell. Denote the region of fluid on cell D_j at time t by

$$V_j(t) \;=\; \{(x,z) : x \in D_j, \; z_{bot}(x) \le z \le z_{top}(x,t)\}. \tag{11}$$

(See Fig. 1.) Let ψ be a smooth function ("test function") defined on D_j. Multiply the x-component (9) by $\psi(x)$ and integrate on the region $V_j(t)$ to obtain

$$\iint_{V_j(t)} \left\{ \frac{\partial u}{\partial t} \;+\; uu_x \;-\; fv \right\} \psi(x)\, dz\, dx \;=\; -\frac{1}{\rho} \iint_{V_j(t)} \frac{\partial P}{\partial x}\, \psi(x)\, dz\, dx. \tag{12}$$

Suitable transformations of this equation will yield a weak form of the momentum equation (9) that can be used to develop discontinuous Galerkin numerical algorithms. Below, the two sides of this equation are addressed separately.
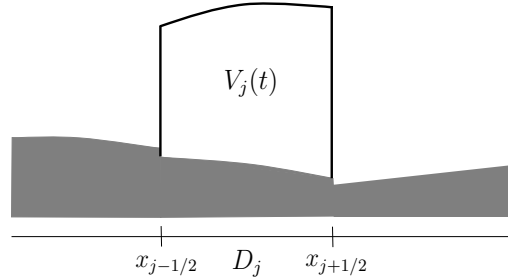
Fig. 1. The region $V_j(t)$ consists of the water column lying on grid cell $D_j = [x_{j-1/2}, \; x_{j+1/2}]$ at time t. The weak form of the momentum equation is obtained by an integration on this region. In this picture, the shaded portion represents bottom topography.

3.1. The left side of Eq. (12)

The left side of Eq. (12) can be represented as

$$\int_{D_j} \left\{ \int_{z_{bot}(x)}^{z_{top}(x,t)} \left[\frac{\partial u}{\partial t} \;+\; uu_x \;-\; fv \right] \psi(x)\, dz \right\} dx$$

$$=\; \int_{D_j} \left[z_{top}(x,t) - z_{bot}(x) \right] \left[\frac{\partial u}{\partial t} \;+\; uu_x \;-\; fv \right] \psi(x)\, dx \tag{13}$$

$$=\; \int_{D_j} h(x,t) \left[u_t \;+\; uu_x \;-\; fv \right] \psi(x)\, dx.$$

The second line of (13) follows from the fact that the integrand for the inner integral in the first line is independent of z. Now multiply the mass conservation equation (4), which is $h_t + (uh)_x = 0$ in this case, by u and combine with the last line in (13) to obtain

$$\int_{D_j} \left\{ \frac{\partial}{\partial t}(hu) + \frac{\partial}{\partial x}\Big[u(hu)\Big] - fhv \right\} \psi(x) \, dx. \tag{14}$$

3.2. A change of dependent variable

At this stage, it is convenient to introduce the following change of dependent variable. For any (x, t), the layer thickness $h(x, t)$ is the volume per unit horizontal area for a water column located at position x at time t. The quantity

$$p_b(x, t) = \rho g h(x, t)$$

is then the weight per unit horizontal area for that water column, and it is thus the difference between the pressure at the bottom of the fluid and the atmospheric pressure at the top of the fluid. For the constant-density shallow water equations, either of the quantities h and p_b could be used as the mass variable, such as in the mass conservation equation (4). However, the quantity p_b appears in the formulation of pressure forcing that is developed below, so for the sake of consistency in notation the quantity h in (14) will be replaced by p_b.

So, multiply the momentum equation (12) by ρg and carry this factor through the subsequent calculations to obtain

$$\int_{D_j} \left\{ \frac{\partial}{\partial t}(p_b u) + \frac{\partial}{\partial x}\Big[u(p_b u)\Big] - f p_b v \right\} \psi(x) \, dx$$

for the left side. An integration by parts yields

$$\int_{D_j} \left\{ \frac{\partial}{\partial t}(p_b u) - f p_b v \right\} \psi(x) \, dx \quad + \quad \Big[u(p_b u)\, \psi(x)\Big]_{x=x_{j-1/2}}^{x=x_{j+1/2}} \quad - \quad \int_{D_j} u(p_b u)\, \psi'(x) \, dx. \tag{15}$$

This expression will be used as the left side of the weak form of the x-component of the momentum equation. The quantities $p_b u$ and $p_b v$ are equal to g times the components of horizontal momentum per unit horizontal area.

In the discussions of multi-layer models in [8] and [9] and in an earlier paper by Bleck and Smith [2], vertical differences of pressure across layers are used to represent two-dimensional mass densities (times g) of those layers. In those works, p_b denotes the vertical sum of those pressure differences. The usage of p_b in the present situation is consistent with that usage, and it aids the process of enforcing consistency between the layer equations and the vertically-integrated barotropic equations, in the case of a multi-layer model.

3.3. Pressure forcing: The right side of Eq. (12)

After the multiplication by ρg that is mentioned in the preceding subsection, the right side of Eq. (12) becomes

$$-g \iint_{V_j(t)} \frac{\partial P}{\partial x} \, \psi(x) \, dz \, dx.$$

Some manipulations and a two-dimensional integration by parts shows that this quantity is equal to

$$-g \iint_{V_j(t)} \left(\frac{\partial}{\partial x}, \frac{\partial}{\partial z} \right) \cdot \left(P, \ 0 \right) \psi(x) \ dz \ dx$$

$$= \ -g \int_{\partial V_j(t)} \left(P, \ 0 \right) \cdot \mathbf{n} \ \psi(x) \ dS \ + \ g \iint_{V_j(t)} \left(P, \ 0 \right) \cdot \left(\frac{\partial}{\partial x}, \frac{\partial}{\partial z} \right) \psi(x) \ dz \ dx$$

$$= \ -g \int_{\partial V_j(t)} \left(P, \ 0 \right) \cdot \mathbf{n} \ \psi(x) \ dS \ + \ g \int_{D_j} \left[\int_{z_{bot}(x)}^{z_{top}(x,t)} P(x,z,t) \ dz \right] \psi'(x) \ dx$$

$$= \ -g \int_{\partial V_j(t)} \left(P, \ 0 \right) \cdot \mathbf{n} \ \psi(x) \ dS \ + \ \int_{D_j} H(x,t) \ \psi'(x) \ dx \qquad (16)$$

where

$$H(x,t) \ = \ g \int_{z_{bot}(x)}^{z_{top}(x,t)} P(x,z,t) \ dz \qquad (17)$$

is the vertically-integrated horizontal pressure force (times g), $\partial V_j(t)$ denotes the boundary of $V_j(t)$, and $\mathbf{n}$ denotes the outward unit normal vector on $\partial V_j(t)$. At the left and right edges of $V_j(t)$, the outward unit normals are $\mathbf{n} = (-1,0)$ and $\mathbf{n} = (1,0)$, respectively. Along the graph of a differentiable function ϕ, the upper unit normal vector at horizontal position x is $(-\phi'(x), 1)/((\phi'(x))^2 + 1)^{1/2}$, and the element of arclength is $((\phi'(x))^2 + 1)^{1/2}dx$. The final line in Eq. (16) can then be expressed as

$$-\Big[H(x,t) \ \psi(x) \Big]_{x=x_{j-1/2}}^{x=x_{j+1/2}} \ + \ \int_{D_j} H(x,t) \ \psi'(x) \ dx$$

$$+ \ g \int_{D_j} p_0 \frac{\partial z_{top}}{\partial x} \ \psi(x) \ dx \ - \ g \int_{D_j} \Big[p_0 + p_b(x,t) \Big] \frac{\partial z_{bot}}{\partial x} \ \psi(x) \ dx \qquad (18)$$

The atmospheric pressure p_0 is the pressure at the top of the region $V_j(t)$, and $p_0 + p_b(x,t)$ is the pressure at the bottom of that region.

In the special case where the test function ψ satisfies $\psi(x) = 1$ for all x, the pressure forcing (18) reduces to g times the integral of $P \, dz$ around the boundary of the fluid region $V_j(t)$. Such an integral, applied to the region between two coordinate surfaces in a variable-density fluid, is the starting point for a method developed by Lin [12] for representing the pressure forcing in finite volume methods.

In the preceding analysis, the atmospheric pressure p_0 could vary with x and t; this property could be relevant, for example, if the shallow water equations are used to model storm surge generated by hurricanes. However, for the remainder of this paper, it will be convenient to assume that p_0 is constant, as this enables some simplification of some of the formulas that follow. The case of variable p_0 can be recovered by making suitable modifications.

If p_0 is constant on grid cell D_j, then $\frac{\partial P}{\partial x} = \frac{\partial}{\partial x}(P - p_0)$ everywhere on the region $V_j(t)$, so P can be replaced with $P - p_0$ throughout the preceding calculation. In that case, the expression (18) can be simplified to

$$-\Big[H(x,t) \ \psi(x) \Big]_{x=x_{j-1/2}}^{x=x_{j+1/2}} \ + \ \int_{D_j} H(x,t) \ \psi'(x) \ dx \ - \ g \int_{D_j} p_b(x,t) \frac{\partial z_{bot}}{\partial x} \ \psi(x) \ dx, \qquad (19)$$

and the definition of $H(x,t)$ in Eq. (17) becomes

$$H(x,t) \; = \; g \int_{z_{bot}(x)}^{z_{top}(x,t)} \left(P(x,z,t) - p_0 \right) \, dz \; = \; g \int_{z_{bot}(x)}^{z_{top}(x,t)} p(x,z,t) \, dz. \tag{20}$$

Here, $p(x,z,t) = P(x,z,t) - p_0$ is the contribution to the pressure at (x,z,t) that is due to the fluid above elevation z; the quantity p varies from 0 at the top of the fluid to p_b at the bottom. In effect, the preceding considerations enable one to disregard the atmospheric pressure during the calculation of the integral form of the pressure forcing.

Section 4 discusses the calculation of the vertically-integrated pressure forcing H at points in the interiors of grid cells and at the edges of grid cells.

The preceding analysis assumes that all functions involved are continuously differentiable on the closed region $V_j(t)$, in order to justify the steps that are taken. An alternative would be to do these calculations on an open subregion and then take one-sided limits at each end of the interval D_j. That approach is taken in the proof of well-balancing in Section 5. In that case, it is essential to be careful with the limits at cell edges, as the computed values of H at cell edges are based on interpolations involving neighboring grid cells.

3.4. Weak forms of the governing equations

The weak form of the x-component (9) of the momentum equation can be obtained by combining the expressions (15) and (19) to yield

$$\int_{D_j} \left\{ \frac{\partial}{\partial t}(p_b u) \; - \; f p_b v \right\} \psi(x) \, dx \quad + \quad \left[u(p_b u) \, \psi(x) \right]_{x=x_{j-1/2}}^{x=x_{j+1/2}} \quad - \quad \int_{D_j} u(p_b u) \, \psi'(x) \, dx$$

$$= \; - \left[H(x,t) \, \psi(x) \right]_{x=x_{j-1/2}}^{x=x_{j+1/2}} \quad + \quad \int_{D_j} H(x,t) \, \psi'(x) \, dx \quad - \quad g \int_{D_j} p_b(x,t) \, \frac{\partial z_{bot}}{\partial x} \, \psi(x) \, dx. \tag{21}$$

Similarly, the weak form of the y-component (10) of the momentum equation is

$$\int_{D_j} \left\{ \frac{\partial}{\partial t}(p_b v) \; + \; f p_b u \right\} \psi(x) \, dx$$

$$+ \quad \left[u(p_b v) \, \psi(x) \right]_{x=x_{j-1/2}}^{x=x_{j+1/2}} \quad - \quad \int_{D_j} u(p_b v) \, \psi'(x) \, dx \quad = \quad 0. \tag{22}$$

In this case, the pressure forcing is zero due to the assumption that all quantities are independent of y. Under that same assumption, the mass equation (4) can be expressed as

$$\frac{\partial p_b}{\partial t} + \frac{\partial}{\partial x}(p_b u) \; = \; 0$$

by using the relation $p_b(x,t) = \rho g h(x,t)$. The weak form of the mass equation is then

$$\int_{D_j} \frac{\partial p_b}{\partial t} \, \psi(x) \, dx \quad + \quad \left[p_b u \, \psi(x) \right]_{x=x_{j-1/2}}^{x=x_{j+1/2}} \quad - \quad \int_{D_j} p_b u \, \psi'(x) \, dx \quad = \quad 0. \tag{23}$$

3.5. A summary of the development of DG methods for this system

From the preceding results, a discontinuous Galerkin numerical method can be developed as follows. For each grid cell, choose a basis for a vector space of polynomials in x on that cell; express each dependent variable as a linear combination of the basis functions, with coefficients that depend on t; in each of the weak forms, let ψ be each of the basis functions; and obtain a system of ordinary differential equations in t for the coefficients of the basis functions in the representations of the dependent variables. An example of a polynomial basis, based on Legendre polynomials, is described in Section 6 of [7]; this basis was also used for the numerical computations that are described in Section 7 of the present paper.

For fixed t, the numerical approximation to each dependent variable is a polynomial in x in each grid cell, with different polynomials being used in different cells and no requirement of continuity across cell edges. In keeping with this philosophy, also represent the elevation z_{bot} of the bottom topography as a polynomial in each grid cell, with no requirement of continuity across cell edges; such a configuration is illustrated in Fig. 1.

An analysis of dispersion relations for the propagation of linear inertia-gravity waves, reported in [7], found that polynomials of degree two produced results that were noticeably better than polynomials of degree one, but polynomials of degree three yielded diminishing returns. Polynomials of degree two are used in the numerical computations described in Section 7, and also in [7], [8], and [9].

Once the spatial discretization is specified, a variety of time-stepping methods can be used for the time integration. The computations that are described in Section 7 use a two-level time-stepping method that is described and analyzed in [7]. This method is based on a time-stepping method for barotropic-baroclinic splitting for multi-layer models, which is specialized to the case of the single-layer shallow water equations for the sake of the present work. In [7] the stability properties of this method are compared to those of some Runge-Kutta time-stepping methods, for the linearized one-dimensional shallow water equations. Compared to the other methods, the two-level method has a more restrictive bound on the time step; for example, in the case of piecewise quadratic spatial approximations, the Courant number $c\Delta t/\Delta x$ can be at most 0.16. However, a lower operation count per time step leads to no disadvantage in efficiency, relative to the other methods. In some experiments with linear inertia-gravity waves reported in [7], the DG method performed at least as well as, and in some cases better, than some standard finite difference methods having looser stability constraints.

As part of the formulation of the numerical method, it is necessary to determine the values of the quantities at $x = x_{j\pm 1/2}$ that are included in Eqs. (21)–(23). The quantities $u(p_b u)$ and $u(p_b v)$ in (21)–(22) are fluxes of momentum due to advection, and the quantity $p_b u$ in (23) is a flux of mass. The quantity H in (21) plays the structural role of a flux, and it can be regarded as a flux of momentum due to pressure forcing. The computation of these quantities at cell edges is discussed in Section 4.2 and Section 6.

4. Calculation of the vertically-integrated pressure forcing H

As in the latter part of Section 3.3, assume that the atmospheric pressure p_0 is constant on grid cell D_j, and use the simplified representation (19) of the pressure forcing, with the definition of $H(x,t)$ given in Eq. (20).

4.1. Values of H in the interiors of grid cells

Assume that x is in the interior of a grid cell. Eq. (20) can then be expressed as

$$
\begin{aligned}
H(x,t) &= g \int_{z_{bot}(x)}^{z_{top}(x,t)} p(x,z,t)\,dz = g \int_{p_b(x,t)}^{0} p\,\frac{\partial z}{\partial p}\,dp = g \int_{p_b(x,t)}^{0} \frac{p}{-\rho g}\,dp \\
&= \int_{0}^{p_b(x,t)} \alpha\,p\,dp \\
&= \frac{1}{2}\,\alpha\left(\,p_b(x,t)\,\right)^2,
\end{aligned}
\tag{24}
$$

where $\alpha = 1/\rho$ is the specific volume (volume per unit mass) of the fluid. This derivation uses the hydrostatic condition $\partial p/\partial z = -\rho g$ and the assumption that the density ρ is constant throughout the fluid.

The following notation will be useful in subsequent discussions. If x is in the interior of a grid cell, let $p_b'(x) = \rho g(z_{top,rest} - z_{bot}(x))$ denote the value of $p_b(x,t)$ at the global rest state consisting of a level free surface and zero velocity; in this notation, the prime ($'$) does not denote a derivative. Then, for an arbitrary fluid state, let $\eta(x,t)$ denote the relative perturbation in $p_b(x,t)$, i.e., $\eta(x,t) = \big(p_b(x,t) - p_b'(x)\big)/p_b'(x)$. Thus

$$
p_b(x,t) = p_b'(x) + (p_b'\eta)(x,t).
\tag{25}
$$

The representation (24) of $H(x,t)$ can then be written as

$$
H(x,t) = \frac{1}{2}\,\alpha\left(\,p_b'(x) + (p_b'\eta)(x,t)\,\right)^2.
\tag{26}
$$

The notation in Eq. (25) was used by Bleck and Smith [2] during the development of a barotropic-baroclinic time splitting for isopycnic-coordinate ocean modeling. In the formula for $p_b'(x)$ that is used above, for the present case of constant density, the terms $z_{top,rest}$ and $z_{bot}(x)$ are specified during the definition of the fluid domain. The quantity $z_{top,rest}$ is a constant (e.g., zero) that specifies the elevation of the free surface at the global rest state, and the elevation $z_{bot}(x)$ of the bottom topography is defined relative to $z_{top,rest}$. In the case of a multi-layer model for a variable-density fluid, $p_b'(x)$ is a sum of vertical pressure increments across all layers, as seen in the global rest state.

The quantity $p_b'\eta$ in Eqs. (25)–(26) is the perturbation in the bottom pressure, relative to the global rest state. Due to the assumption of constant density, $p_b'\eta$ is also equal to ρg times the perturbation in the elevation of the free surface. This follows from observing that $p_b = \rho g(z_{top} - z_{bot})$ and $p_b' = \rho g(z_{top,rest} - z_{bot})$, so $p_b'\eta = p_b - p_b' = \rho g(z_{top} - z_{top,rest})$.

4.2. Values of H at the edges of grid cells

In the weak form (21) of the x-component of the momentum equation on grid cell D_j, the pressure forcing includes values of $H(x,t)$ at the cell edges $x_{j\pm1/2}$. For these values, it generally does not suffice to use one-sided limits of H from within the interior of D_j, for the following reason.

In a piecewise polynomial representation of the solution, as obtained with a DG method, the pressure perturbation $p_b'\eta$, at a fixed time, need not be continuous across cell edges. Equivalently, the elevation of the free surface need not be continuous across cell edges. An example is illustrated in Fig. 2. The configuration in the Figure is not physically realizable, in literal terms; instead, the Figure illustrates a piecewise polynomial that serves as a numerical approximation to an exact solution.
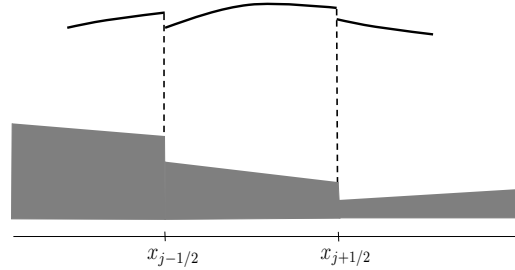
Fig. 2. This figure shows a piecewise polynomial approximation to the free surface in adjacent grid cells, at a fixed time. This approximation need not be continuous across cell edges, due to the nature of discontinuous Galerkin methods. The discontinuities imply that one-sided limits are not suitable for computing pressure forcing at cell edges.

If such a numerical approximation is used to compute pressure forcing at cell edges, then a discontinuity in $p_b'\eta$ creates a problem. Consider any fixed elevation z where the fluids in cells D_{j-1} and D_j are in contact, as represented in the numerical solution. A computed pressure at that elevation on the right side of the edge would be different from the computed pressure at that same elevation on the left side, as the elevation z is at different distances below the free surface on the two sides of the edge. Integrals of pressure over a given vertical line segment would then be different on the two sides. If such integrals are used, in some way or another, to compute pressure forcing at that cell edge, then the numerical algorithm could produce different values for the net pressure force exerted by the fluid in cell D_{j-1} on the fluid in cell D_j and the net pressure force exerted by cell D_j on cell D_{j-1}. That is, the numerical method could violate Newton's Third Law, which states that when two bodies exert forces on each other, the two forces must have equal magnitudes and opposite directions. Similar concerns were expressed by Lin [12] during the development of integral forms of pressure forcing for finite volume methods.

It is therefore necessary to use some sort of interpolation of the one-sided limits of free-surface elevation on either side of the edge $x_{j-1/2}$ to produce a common value that can be used to compute the pressure forcing at the left edge of cell D_j and also at the right edge of cell D_{j-1}. Interpolating the perturbations in the elevation of the free surface is equivalent to interpolating the bottom-pressure perturbation $p_b'\eta$.

One particular method for interpolating $p'_b\eta$ is discussed in Section 6. For now, assume that $p'_b\eta$ has been interpolated by some means or another, and denote the interpolated value at edge $x_{j-1/2}$ by $(p'_b\eta)_{j-1/2}$.

It was assumed in Section 3.5 that the bottom elevation z_{bot} is a polynomial in each grid cell, with no requirement that z_{bot} be continuous across cell edges. Then $p'_b = \rho g(z_{top,rest} - z_{bot})$ is also a polynomial in each grid cell. At cell edge $x_{j-1/2}$, let $p'_b(x^-_{j-1/2})$ and $p'_b(x^+_{j-1/2})$ denote the left and right limits, respectively, of p'_b. Then let

$$
\begin{aligned}
\hat{H}^+_{j-1/2} &= \frac{1}{2}\alpha\left[\, p'_b(x^+_{j-1/2}) + (p'_b\eta)_{j-1/2}\,\right]^2 \\
\hat{H}^-_{j-1/2} &= \frac{1}{2}\alpha\left[\, p'_b(x^-_{j-1/2}) + (p'_b\eta)_{j-1/2}\,\right]^2,
\end{aligned}
\tag{27}
$$

in analogy to the representation (26) of $H(x,t)$ for the case where x is in the interior of a grid cell. In the numerical method, the quantity $\hat{H}^+_{j-1/2}$ serves as a value of H at edge $x_{j-1/2}$ for usage in cell D_j, and the quantity $\hat{H}^-_{j-1/2}$ serves as a value of H at edge $x_{j-1/2}$ for usage in cell D_{j-1}.

The quantities $\hat{H}^+_{j-1/2}$ and $\hat{H}^-_{j-1/2}$ are illustrated in Fig. 3 and can be interpreted as follows. Interpolating the pressure perturbation $p'_b\eta$ at the bottom of the fluid is equivalent to interpolating the perturbation in the elevation of the free surface at the top of the fluid. In accordance with the comment at the end of Section 4.1, define an interpolated free-surface perturbation $(\Delta z)_{j-1/2}$ by $(p'_b\eta)_{j-1/2} = \rho g(\Delta z)_{j-1/2}$, and let $(z_{top})_{j-1/2} = z_{top,rest} + (\Delta z)_{j-1/2}$ denote the corresponding interpolated elevation. A calculation analogous to (24) and (26) shows that

$$
\begin{aligned}
\hat{H}^+_{j-1/2} &= g\int_{z_{bot}(x^+_{j-1/2})}^{(z_{top})_{j-1/2}} p(x_{j-1/2}, z, t)\,dz \\
\hat{H}^-_{j-1/2} &= g\int_{z_{bot}(x^-_{j-1/2})}^{(z_{top})_{j-1/2}} p(x_{j-1/2}, z, t)\,dz.
\end{aligned}
$$

If the bottom topography is discontinuous at the edge $x_{j-1/2}$, then the difference between $\hat{H}^+_{j-1/2}$ and $\hat{H}^-_{j-1/2}$ is g times the vertically-integrated pressure along the sidewall at that edge. The computations on the two sides of the cell edge are therefore in agreement about the forces exerted by the fluid in one cell on the fluid in the other cell, over the vertical extent on which the two water masses are in direct contact, as represented in the numerical solution. The numerical representation of pressure forcing at cell edges thus satisfies Newton's Third Law.

The pressure forcing terms on the right side of the weak form (21) of the x-component of the momentum equation are then implemented as

$$
-\left[\hat{H}^-_{j+1/2}\,\psi(x^-_{j+1/2}) \;-\; \hat{H}^+_{j-1/2}\,\psi(x^+_{j-1/2})\right] \;+\; \int_{D_j} H(x,t)\,\psi'(x)\,dx
$$

$$
-\; g\int_{D_j} p_b(x,t)\,\frac{\partial z_{bot}}{\partial x}\,\psi(x)\,dx.
\tag{28}
$$

Here, $\psi(x^-_{j+1/2})$ and $\psi(x^+_{j-1/2})$ are one-sided limits of the test function ψ in cell D_j.
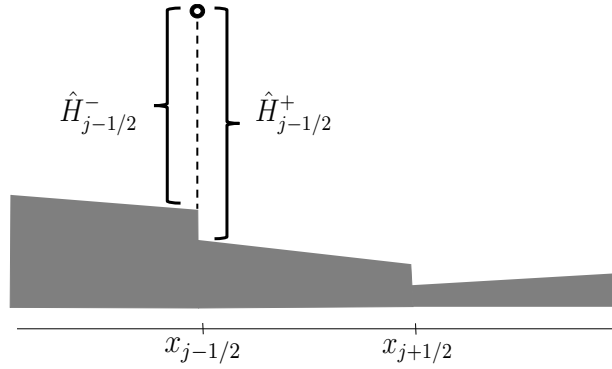
Fig. 3. An illustration of the vertically-integrated pressure forcings $\hat{H}^{+}_{j-1/2}$ and $\hat{H}^{-}_{j-1/2}$ on each side of cell edge $x_{j-1/2}$. Each of these quantities is g times an integral of pressure over the vertical interval that is indicated by a bracket. In this Figure, the small circle at the top of the vertical dashed line segment represents the elevation $(z_{top})_{j-1/2}$ that results from the interpolation of $p'_b\eta$ at the cell edge.

4.3. An assumption about the interpolation of $p'_b\eta$ at cell edges

A method for computing the interpolated value $(p'_b\eta)_{j-1/2}$ at cell edge $x_{j-1/2}$ has not yet been specified, as of this stage in this paper. However, for purposes of the discussion of well-balancing in Section 5, it is necessary to impose a modest assumption regarding any method for performing the interpolation.

Assumption. If, for fixed t, the function $p'_b\eta$ is continuous in x across cell edge $x_{j-1/2}$, and if the momentum density $p_b u$ is also continuous at that edge, then it is assumed here that the interpolated value $(p'_b\eta)_{j-1/2}$ is equal to the common value of the left and right limits of $p'_b\eta$. That is,

$$(p'_b\eta)_{j-1/2} \quad = \quad \lim_{x \to x^{+}_{j-1/2}} (p'_b\eta)(x,t) \quad = \quad \lim_{x \to x^{-}_{j-1/2}} (p'_b\eta)(x,t). \tag{29}$$

One might expect that if $p'_b\eta$ is continuous at an edge, then the interpolated value of that quantity should be the value of that continuous function at that edge. However, the interpolation method developed in Section 6 uses a Riemann problem whose solution also includes information about $p_b u$, and this is why $p_b u$ is also mentioned in the Assumption.

The condition (29) is an analogue of a consistency condition that is imposed on finite volume methods for conservation laws of the form $q_t + f(q)_x = 0$; in this setting, a numerical flux $F(Q_{j-1}, Q_j)$ at cell edge $x_{j-1/2}$ is typically assumed to be consistent with the physical flux f, in the sense that $F(Q, Q) = f(Q)$ for all Q. See, e.g., LeVeque [10].

If the Assumption is satisfied, then the quantity $\hat{H}^{+}_{j-1/2}$ in Eq. (27) satisfies

$$
\begin{aligned}
\hat{H}^{+}_{j-1/2} \quad &= \quad \frac{1}{2}\alpha \left[\, p'_b(x^{+}_{j-1/2}) + (p'_b\eta)_{j-1/2} \,\right]^2 \\
&= \quad \frac{1}{2}\alpha \left[\, p'_b(x^{+}_{j-1/2}) + \lim_{x \to x^{+}_{j-1/2}} (p'_b\eta)(x,t) \,\right]^2 \\
&= \quad \lim_{x \to x^{+}_{j-1/2}} \frac{1}{2}\alpha \left[\, p'_b(x) + (p'_b\eta)(x,t) \,\right]^2 \\
&= \quad \lim_{x \to x^{+}_{j-1/2}} H(x,t).
\end{aligned}
\tag{30}
$$

The last line in Eqs. (30) relies on the expression in Eq. (26) for $H(x,t)$ in the interiors of grid cells. Similarly, if the Assumption is satisfied at cell edge $x_{j+1/2}$, then

$$\hat{H}^-_{j+1/2} \quad = \quad \lim_{x \to x^-_{j+1/2}} H(x,t). \tag{31}$$

Now assume that $p'_b \eta$ and $p_b u$ are continuous on an open interval that contains the grid cell $D_j = [x_{j-1/2}, x_{j+1/2}]$. In this special case, the values of $\hat{H}^+_{j-1/2}$ and $\hat{H}^-_{j+1/2}$ that are used at the cell edges $x_{j\pm1/2}$ in the pressure forcing (28) are, in fact, one-sided limits of $H(x,t)$ from within the interior of D_j.

5. Well-balanced forcing

The standard representation of the pressure forcing for the shallow water equations, as outlined in Section 2.1, contains time-independent terms that involve spatial derivatives of the elevation of the bottom topography. These terms can lead to numerical methods that are not well-balanced, as described in Section 2.2, so special steps may become necessary in order to avoid this problem. On the other hand, it will be shown here that the alternate representation developed in Section 3 is well-balanced without any additional effort, subject to the Assumption stated in Section 4.3.

Theorem. Assume that the atmospheric pressure p_0 is constant and that the free-surface elevation is constant on an open interval that contains the grid cell $D_j = [x_{j-1/2}, x_{j+1/2}]$; the latter statement is equivalent to assuming that the bottom-pressure perturbation $p'_b \eta$ is constant on that open interval. Also assume that the momentum density $p_b u$ is continuous on that open interval and that the Assumption stated in Section 4.3 is satisfied. Then the pressure forcing expressed in Eq. (28) is zero.

Remarks.

(1) The first and last sentences in the statement of the theorem constitute a definition of the term "well-balanced" as used in the present context. The pressure forcing (28) is the forcing that is actually implemented for numerical computations.

(2) If the velocity u is zero everywhere, then the hypothesis about continuity of the momentum density $p_b u$ is satisfied, and the Assumption in Section 4.3 reduces to a statement that the interpolation method for $p'_b \eta$ reproduces the continuous values when this function is continuous at cell edges.

(3) Two integrals appear in Eq. (28), and for purposes of the theorem, those integrals should be interpreted as exact values. However, in an implementation of a DG method, those integrals are computed with a quadrature method. If the integrals are not computed exactly, for some reason, then the quadrature errors should be taken into account when interpreting the conclusion of the theorem. Bonev et al. [3] discuss the possibility of inexact integration in problems with two horizontal dimensions, in a case where the formulation of pressure forcing includes the gradient of bottom topography.

Proof of the theorem.

Let $\epsilon > 0$, with ϵ less than half the length of grid cell D_j. Let $D^\epsilon_j = [x_{j-1/2} + \epsilon, x_{j+1/2} - \epsilon]$ denote the subinterval of D_j obtained by moving inward by distance ϵ from each endpoint. Denote the region of fluid

on the subinterval D_j^ϵ by $V_j^\epsilon(t) = \{(x,z) : x \in D_j^\epsilon, \; z_{bot}(x) \le z \le z_{top}(x,t)\}$.

Now assume that the elevation z_{top} of the free surface is constant on an open interval that contains D_j. The pressure P within the fluid satisfies $P(x,z,t) = p_0 + \rho g(z_{top} - z)$, so $\partial P/\partial x = 0$ on the region $V_j(t)$ defined in Eq. (11). A calculation analogous to the one in Section 3.3 shows

$$
\begin{aligned}
0 &= -g \iint_{V_j^\epsilon(t)} \frac{\partial}{\partial x}\left(P - p_0\right) \psi(x) \, dz \, dx \\[2mm]
&= -\Big[H(x,t)\,\psi(x) \Big]_{x=(x_{j-1/2})+\epsilon}^{x=(x_{j+1/2})-\epsilon} \quad + \quad \int_{D_j^\epsilon} H(x,t)\,\psi'(x)\,dx \\[2mm]
&\qquad - g \int_{D_j^\epsilon} p_b(x,t)\, \frac{\partial z_{bot}}{\partial x}\,\psi(x)\,dx.
\end{aligned}
\tag{32}
$$

The only difference between this result and Eq. (19) is that the latter relies on integration on the fluid region $V_j(t)$ and the interval D_j, whereas the present result uses $V_j^\epsilon(t)$ and D_j^ϵ.

Eq. (32) holds for every $\epsilon > 0$ that is less than half the length of cell D_j. Now consider the limit as $\epsilon \to 0^+$. One of the hypotheses of the theorem is that the function $p_b'\eta$ is constant on an open interval containing the grid cell D_j, so $p_b'\eta$ is continuous at each of the end points $x_{j-1/2}$ and $x_{j+1/2}$. The Assumption stated in Section 4.3 is also assumed to hold here. The discussion in Section 4.3 then implies that Eqs. (30) and (31) are satisfied in the present situation; these equations can be expressed as

$$
\begin{aligned}
\lim_{\epsilon \to 0^+} H\Big((x_{j-1/2}) + \epsilon, t\Big) &= \hat{H}_{j-1/2}^+ \\[2mm]
\lim_{\epsilon \to 0^+} H\Big((x_{j+1/2}) - \epsilon, t\Big) &= \hat{H}_{j+1/2}^- \; .
\end{aligned}
\tag{33}
$$

Now let $\epsilon \to 0^+$ in Eq. (32) and combine with Eqs. (33) to obtain

$$
\begin{aligned}
0 &= -\Big[\hat{H}_{j+1/2}^-\,\psi(x_{j+1/2}^-) \;-\; \hat{H}_{j-1/2}^+\,\psi(x_{j-1/2}^+) \Big] \quad + \quad \int_{D_j} H(x,t)\,\psi'(x)\,dx \\[2mm]
&\qquad - g \int_{D_j} p_b(x,t)\, \frac{\partial z_{bot}}{\partial x}\,\psi(x)\,dx.
\end{aligned}
\tag{34}
$$

The right side of this equation is the same as the expression in (28), and it is the representation of the pressure forcing that is actually implemented in a numerical method. This representation of the pressure forcing is zero, so the numerical method is well-balanced. This completes the proof. □

Remark.

The basic idea of the proof is that the formula (28) for the pressure forcing is obtained by manipulating the integral

$$
-g \iint_{V_j(t)} \frac{\partial}{\partial x}\left(P - p_0\right) \psi(x) \, dz \, dx.
$$

If the free surface is level on the grid cell D_j, then the integrand is zero. The formula (28), which is what is actually implemented, would presumably then be zero. However, it is necessary to be careful at the cell edges, and that is why the parameter ϵ is introduced.

6. Interpolations at the edges of grid cells

The weak form (21) of the x-component of the momentum equation includes values of the vertically-integrated horizontal pressure force H at the edges of grid cells. As noted in Section 4.2, the computation of these values requires an interpolation of the bottom-pressure perturbation $p'_b\eta$ at each cell edge. In addition, the weak form (23) of the mass equation includes values of the mass flux $p_b u$ at cell edges, so this quantity should also be interpolated. The quantity $p_b u$ also serves as a momentum density, and it thus plays a role in the momentum flux $u(p_b u)$, which appears in the momentum equation (21).

A standard method for computing values of dependent variables at a cell edge is to solve a Riemann problem (LeVeque [9]), in which the one-sided limits of those variables at the cell edge are used to define piecewise constant initial data. The solution resulting from that initial state is then evaluated at the edge. The one-sided limits are thus interpolated according to the dynamics of a system of partial differential equations, as opposed to some sort of simple averaging.

6.1. Formulation of the governing equations

The Riemann problem considered here uses the one-dimensional shallow water equations, linearized to represent small perturbations of a rest state. This linearized system does not include all situations in which the shallow water equations are used; rather, a linearized system is used here partly for the sake of simplicity and partly for its relevance to barotropic-baroclinic time splitting for multi-layer ocean circulation models having multiple time scales ([6], [8]). In such a splitting, the fast external motions are modeled by a lower-dimensional, vertically-integrated system that is similar to the shallow water equations. The dynamics of such a system are nearly linear; for example, the maximum fluid speed is on the order of one meter per second, whereas the speed of external gravity waves can be on the order of 100 to 200 meters per second. Also, the maximum perturbation in the elevation of the free surface is on the order of one meter, but the depth of the fluid is on the order of hundreds or thousands of meters. It is therefore hypothesized here that a linear Riemann problem is adequate for interpolations of $p'_b\eta$ and $p_b u$ at cell edges, for the case of the vertically-integrated portion of a barotropic-baroclinic splitting. That case is a major motivation for the discussions in the present paper.

For the linearized system used here, it is also assumed that the Coriolis parameter f is zero, as solutions of the Riemann problem are of interest only in a neighborhood of a cell edge and for short times after the piecewise constant initial state is imposed. Loosely speaking, the effect of rotation in the shallow water system is felt on a length scale given by the Rossby radius of deformation c/f, where c is the speed of external gravity waves (Gill [5], Vallis[15]). If $c = 100$ m/s and f has the mid-latitude value 10^{-4} s^{-1}, then $c/f = 10^6$ m $= 10^3$ km.

To formulate the linearized system for the present analysis, consider a horizontal spatial interval on which the bottom boundary of the fluid is level; this hypothesis will be applied to each side of a cell edge at which interpolations are to be performed. For an interval on which the bottom boundary is level, let

D denote the constant depth of the fluid at the rest state, and let $\delta(x,t)$ denote the perturbation in the elevation of the free surface from that state. As in Section 4.1, let $\eta(x,t)$ denote the relative perturbation in $p_b(x,t)$ from the rest value $p_b'(x)$. In the present situation, $p_b'(x)$ has the constant value $\rho g D$, and, as noted in Section 4.1, the perturbation in $p_b(x,t)$ is $p_b(x,t) - p_b'(x) = \rho g \delta(x,t)$. Therefore

$$\eta(x,t) = \frac{\rho g \delta(x,t)}{\rho g D} = \frac{\delta(x,t)}{D},$$

so $\eta(x,t)$ is also equal to the relative perturbation in the thickness of the fluid layer. For the present linear analysis, assume that $|\eta| \ll 1$ and that the horizontal components of velocity are small.

In the case of one horizontal dimension with $f = 0$, the shallow water system (2)–(4) can be expressed as

$$\frac{\partial u}{\partial t} + u u_x = -g\frac{\partial \delta}{\partial x}$$

$$\frac{\partial h}{\partial t} + \frac{\partial}{\partial x}(uh) = 0.$$

The y-component of the momentum equation is not included here, due to the absence of a Coriolis term. In the present case, the layer thickness is $h(x,t) = D + \delta(x,t)$, and the corresponding flux is $uh = (D + \delta)u$. Now regard the products of small quantities as negligible and delete such terms to obtain the linear system

$$\frac{\partial u}{\partial t} = -g\frac{\partial \delta}{\partial x} \tag{35}$$

$$\frac{\partial \delta}{\partial t} + D\frac{\partial u}{\partial x} = 0. \tag{36}$$

The purpose of the present discussion is to develop a method for interpolating values of the pressure perturbation $p_b'\eta$ and the mass flux (or momentum density) $p_b'u$ at cell edges. However, according to Eq. (25), $p_b u = p_b'(1 + \eta)u$. This linearizes to the quantity $p_b'u$ in the present circumstances. So, the system (35)–(36) will next be transformed so that the dependent variables are $p_b'\eta$ and $p_b'u$.

The right side of Eq. (35) is

$$-g\frac{\partial \delta}{\partial x} = -gD\frac{\partial}{\partial x}\left(\frac{\delta}{D}\right) = -c^2\frac{\partial \eta}{\partial x},$$

where $c = \sqrt{gD} = \sqrt{\alpha(\rho g D)} = \sqrt{\alpha p_b'}$, with $\alpha = 1/\rho$. In addition, the mass equation (36) is equivalent to $\eta_t + u_x = 0$. After multiplication by the constant quantity $p_b' = \rho g D$, the system (35)–(36) becomes

$$\frac{\partial}{\partial t}\left(p_b'u\right) = -c^2\frac{\partial}{\partial x}\left(p_b'\eta\right)$$

$$\frac{\partial}{\partial t}\left(p_b'\eta\right) + \frac{\partial}{\partial x}\left(p_b'u\right) = 0.$$

In order to simplify the notation in subsequent calculations, let $U(x,t) = p_b'u(x,t)$ and $E(x,t) = p_b'\eta(x,t)$. The system can then be written as

$$\frac{\partial}{\partial t}\left(\frac{U}{c}\right) + c\frac{\partial E}{\partial x} = 0 \tag{37}$$

$$\frac{\partial E}{\partial t} + c\frac{\partial}{\partial x}\left(\frac{U}{c}\right) = 0. \tag{38}$$

Addition and subtraction produces the characteristic equations

$$\frac{\partial}{\partial t}\left(\frac{U}{c}+E\right) \;+\; c\frac{\partial}{\partial x}\left(\frac{U}{c}+E\right) \;=\; 0 \tag{39}$$

$$\frac{\partial}{\partial t}\left(\frac{U}{c}-E\right) \;-\; c\frac{\partial}{\partial x}\left(\frac{U}{c}-E\right) \;=\; 0. \tag{40}$$

Eq. (39) implies that the quantity $U/c + E$ is constant on characteristic curves $(x(t), t)$ for which $x'(t) = c$, and Eq. (40) implies that $U/c - E$ is constant along characteristic curves for which $x'(t) = -c$. The quantities U/c and E each have units of pressure.

6.2. Formulation of the Riemann problem

Now define a Riemann problem for interpolating dependent variables at cell edge $x_{j-1/2}$ at some time level t_n during the course of a numerical computation. The goal is to compute forcing terms at that time level. In the following discussion, the variable $\tau = t - t_n$ is a time-like variable associated with the Riemann problem that is used to perform the interpolation, with $\tau = 0$ corresponding to $t = t_n$. Evolution of the solution of the Riemann problem with respect to τ for $\tau > 0$ does not, in general, coincide with the evolution of the overall system with respect to t for $t > t_n$. In the following discussion, the systems (37)–(38) and (39)–(40) are modified slightly by replacing t with τ.

The formulation used here allows the possibility of a discontinuity in bottom topography at $x_{j-1/2}$; compared to the case of continuous topography, allowing a discontinuity requires little additional effort, so it is included here as a possibility. Assume that, at the rest state, the fluid has a constant depth D_- for $x < x_{j-1/2}$ and a constant depth D_+ for $x > x_{j-1/2}$, and denote corresponding characteristic velocities by $c_- = \sqrt{gD_-}$ for $x < x_{j-1/2}$ and $c_+ = \sqrt{gD_+}$ for $x > x_{j-1/2}$. The solution of a Riemann problem is used only locally; the other cell edges are not relevant in this process and therefore are not included in the formulation of this problem. The system (37)–(38) (equivalently, (39)–(40)) holds on each of the intervals $(-\infty, x_{j-1/2})$ and $(x_{j-1/2}, +\infty)$, with $c = c_-$ for $x < x_{j-1/2}$ and $c = c_+$ for $x > x_{j-1/2}$. Piecewise constant initial conditions are imposed at time $\tau = 0$, and the resulting solutions on the intervals $(-\infty, x_{j-1/2})$ and $(x_{j-1/2}, +\infty)$ are matched at $x_{j-1/2}$, for $\tau > 0$, by imposing the following interface conditions.

(i) The elevation of the free surface must be continuous at $x_{j-1/2}$ for $\tau > 0$; equivalently, the pressure perturbation $p'_b\eta$ must be continuous at that edge. Otherwise, for reasons stated in Section 4.2, solutions of the system could embody violations of Newton's Third Law.

(ii) The mass flux $p_b u$ must be continuous at $x_{j-1/2}$ for $\tau > 0$, since otherwise the edge can act as a point source or sink of mass. In the present setting, $p_b u$ linearizes to $p'_b u$.

The interface conditions (i) and (ii) can be expressed in terms of one-sided limits as

$$E(x^-_{j-1/2}, \tau) = E(x^+_{j-1/2}, \tau) \qquad \text{and} \qquad U(x^-_{j-1/2}, \tau) = U(x^+_{j-1/2}, \tau), \tag{41}$$

respectively, for $\tau > 0$.

For initial conditions for the system (37)–(38), use

$$U(x,0) = U_L = (p_b'u)_L, \qquad x < x_{j-1/2}$$

$$E(x,0) = E_L = (p_b'\eta)_L, \qquad x < x_{j-1/2}$$

$$U(x,0) = U_R = (p_b'u)_R, \qquad x > x_{j-1/2}$$

$$E(x,0) = E_R = (p_b'\eta)_R, \qquad x > x_{j-1/2}, \tag{42}$$

where the second argument in $U(x,0)$ and $E(x,0)$ refers to $\tau = 0$. Here, the initial values U_L, E_L, U_R, E_R are constants. In practice, these values would be left and right limits of values of $p_b u$ and $p_b'\eta$ in the adjacent grid cells; these values would have been computed by a DG method for time $t = t_n$ during the course of a numerical computation. Due to the intrinsic nature of DG methods, the dependent variables need not be continuous across cell edges, so the initial values in Eqs. (42) need not satisfy the interface conditions in Eqs. (41). An effect of using the Riemann problem is to interpolate the data in (42) so as to give results that do satisfy the interface conditions for $\tau > 0$. To express this another way, the interface conditions (i) and (ii) are statements of balance; the DG method can produce data that are out of balance at cell edges, and the role of the Riemann problem is to adjust the data to obtain such a balance.

6.3. Solution of the Riemann problem

The goal of the present subsection is to find the solution, evaluated at position $x = x_{j-1/2}$, of the system (37)–(38) (equivalently, (39)–(40)) with t replaced by τ, subject to the interface conditions (41) and the initial conditions (42).

Denote the one-sided limits of U and E at $x_{j-1/2}$ by

$$U_-(\tau) = U(x_{j-1/2}^-, \tau), \qquad U_+(\tau) = U(x_{j-1/2}^+, \tau)$$

$$E_-(\tau) = E(x_{j-1/2}^-, \tau), \qquad E_+(\tau) = E(x_{j-1/2}^+, \tau)$$

for all $\tau > 0$. As noted after Eqs. (39)–(40), the quantities $(U/c) + E$ and $(U/c) - E$ are constant along characteristics having velocities c and $-c$, respectively. At position $x_{j-1/2}$, the quantity $(U/c_-) + E$ is therefore determined by initial data for $x < x_{j-1/2}$, and the quantity $(U/c_+) - E$ is determined by initial data for $x > x_{j-1/2}$. These facts, combined with the initial conditions (42), imply

$$\frac{U_-(\tau)}{c_-} + E_-(\tau) = \frac{U_L}{c_-} + E_L \tag{43}$$

$$\frac{U_+(\tau)}{c_+} - E_+(\tau) = \frac{U_R}{c_+} - E_R \tag{44}$$

for all $\tau > 0$. In addition, the interface conditions (41) imply $U_-(\tau) = U_+(\tau)$ and $E_-(\tau) = E_+(\tau)$, so U and E are well-defined at $x_{j-1/2}$. Denote their values at $x_{j-1/2}$ by

$$(p_b'u)_{j-1/2} = U_{j-1/2} = U_- = U_+ \tag{45}$$

$$(p_b'\eta)_{j-1/2} = E_{j-1/2} = E_- = E_+; \tag{46}$$

in these equations, dependences with respect to τ are not included in the notation, as the next results show that the quantities in (45) and (46) are independent of τ. Some algebraic manipulations of Eqs. (43) and (44) yield

$$(p_b'\eta)_{j-1/2} \;=\; \left(\frac{c_-}{c_- + c_+}\right)(p_b'\eta)_L \;+\; \left(\frac{c_+}{c_- + c_+}\right)(p_b'\eta)_R \;+\; \left(\frac{1}{c_- + c_+}\right)\left[\,(p_b'u)_L - (p_b'u)_R\,\right] \quad (47)$$

$$(p_b'u)_{j-1/2} \;=\; \left(\frac{c_+}{c_- + c_+}\right)(p_b'u)_L \;+\; \left(\frac{c_-}{c_- + c_+}\right)(p_b'u)_R \;+\; \left(\frac{c_- c_+}{c_- + c_+}\right)\left[\,(p_b'\eta)_L - (p_b'\eta)_R\,\right]. \quad (48)$$

The value of $(p_b'\eta)_{j-1/2}$ given in Eq. (47) can be used for the computation of the vertically-integrated pressure forcing H at cell edges, as described in Section 4.2.

The quantity $p_b'u$ in Eqs. (47)–(48) is a linearization of the quantity p_bu that is used in the weak forms (21)–(23) of the shallow water equations. In the following discussion, it is assumed that p_bu and $p_b'u$ are used interchangeably. In the weak form (23) of the mass equation, the quantity p_bu serves as a mass flux, and the interpolated values of this quantity can be used in the terms in (23) that are evaluated at cell edges. In the weak form (21) of the x-component of the momentum equation, the quantity p_bu serves as a momentum density; for values of the momentum flux $u(p_bu)$ at cell edges, use the interpolated values of p_bu and averages of one-sided limits of the velocity u. For values of the momentum flux $u(p_bv)$ at cell edges for the y-component (22), use an average of one-sided limits of u and upwind values of p_bv.

6.4. Verification of well-balanced forcing

The theorem on well-balanced forcing that is proved in Section 5 relies on the Assumption that is stated in Section 4.3, namely, that if the functions $p_b'\eta$ and p_bu are continuous at cell edge $x_{j-1/2}$, then the interpolated value $(p_b'\eta)_{j-1/2}$ is equal to the common value of the left and right limits of $p_b'\eta$.

In the present setting, the initial values in Eqs. (42) for the Riemann problem are left and right limits of dependent variables as computed by a DG method at some time level during the course of a computation. A statement that $p_b'\eta$ and p_bu are continuous at $x_{j-1/2}$ can be expressed as $E_L = E_R$ and $U_L = U_R$, i.e., $(p_b'\eta)_L = (p_b'\eta)_R$ and $(p_b'u)_L = (p_b'u)_R$. In this case, Eq. (47) reduces to

$$(p_b'\eta)_{j-1/2} \;=\; (p_b'\eta)_L \;=\; (p_b'\eta)_R. \tag{49}$$

The present interpolation method therefore satisfies the Assumption in Section 4.3, so the resulting representation of the horizontal pressure forcing is well-balanced.

7. Numerical computations

This section describes the results of some numerical computations that test the ideas developed in the previous sections of this paper. One set of computations illustrates the well-balancing that has just been demonstrated. The other computations test the ability of the method to model the propagation of traveling waves across a region with variable bottom topography.

In each of these computations, the fluid is assumed to occupy an infinite straight channel in the y-direction, and all quantities are assumed to be independent of y. Let L denote the width of the channel, and let x be the cross-channel coordinate, with $0 \leq x \leq L$. Solid-wall boundary conditions are imposed at the boundaries $x = 0$ and $x = L$. The weak forms of the mass and momentum equations, as stated in Section 3.4, are discretized with a discontinuous Galerkin numerical method according to the outline given in Section 3.5. Values of fluxes at cell edges are determined by the methods that are specified at the end of Section 6.3. Piecewise polynomials of degree two in x are used to approximate each of the dependent variables, for reasons mentioned in Section 3.5.

The test of well-balancing described in Section 7.1.2 includes wind stress at the top of the fluid and frictional stress along the bottom of the fluid. These stresses are implemented by adding terms of the form

$$g \int_{D_j} \big[\tau_{wind}(x,t) - \tau_{bot}(x,t) \big] \psi(x) \, dx \qquad (50)$$

to the right sides of the x-component (21) and y-component (22) of the weak forms of the momentum equations. (See [7].) In the notation used in (50), the terms τ_{wind} and τ_{bot} refer to the appropriate components of wind stress and bottom stress, respectively; each stress represents a horizontal force per unit horizontal area. The vector form of the bottom stress is represented here as $\rho c_D |\mathbf{u}| \mathbf{u}$, where $\mathbf{u} = (u, v)$ is the horizontal velocity vector and $c_D = 0.003$ is a dimensionless drag coefficient (Bleck and Smith [2]). This formulation follows a sign convention that a stress is the horizontal force per unit horizontal area exerted by an upper region on a lower region, so a minus sign is included in the integral (50). In the present test, the specific volume of the fluid is assumed to be $\alpha = 1/\rho = 0.975 \times 10^{-3} \mathrm{m}^3/\mathrm{km}$.

7.1. Tests of well-balanced forcing

Two tests of well-balancing are described here. For these tests, the infinite straight channel has a trapezoidal cross-section that is symmetric about the midpoint of the interval $[0, L]$; see the top frame in Fig. 4. In this case, $L = 500$ km, and the interval $[0, L]$ is partitioned into 50 grid cells having uniform width $\Delta x = 10$ km. At the endpoints of the spatial interval, the depth of the fluid at the rest state is 10 meters. On the subinterval $0.25L \leq x \leq 0.75L$, the depth has the constant value 1000 meters. Elsewhere, the cell averages of bottom elevation vary linearly; the slope within each cell is equal to half the rate of variation of the cell averages, so the bottom topography is discontinuous across cell edges on this portion of the spatial domain. These discontinuities are introduced deliberately in order to test the behavior of the algorithm in the presence of such discontinuities. For this computation, the Coriolis parameter is $f = 10^{-4} \, \mathrm{s}^{-1}$, which is approximately the value found at latitude 45°N on the earth.

The time increment Δt is determined as follows. On the deepest part of the fluid region, the speed of gravity waves is $c = \sqrt{gD}$, where $D = 1000 \, \mathrm{m}$ and $g = 9.81 \, \mathrm{m/s}^2$; thus $c \approx 99 \, \mathrm{m/s}$. For the two-level time-stepping method discussed in Section 3.5, stability requires the condition $c \Delta t / \Delta x < 0.16$ for the case of the piecewise quadratic spatial approximations that are used here. The present computations use $\Delta x = 10$ km, so Δt was chosen to be 16 seconds.

7.1.1. Static test

For the first test of well-balancing, the system is initially at a rest state, i.e., the components u and v of horizontal velocity are zero, and the free surface at the top of the fluid is level. The wind stress at the top of the fluid and the frictional stress at the bottom of the fluid are both set to zero for all (x, t). The system is then solved for 500 model days, which in this case is equivalent to $2,700,000$ time steps. At the end of that time period, the maximum of the computed values of $|u|$, over the entire spatial domain, is approximately 1.0×10^{-12} meters per second; the maximum computed value of $|v|$ is $\approx 7.2 \times 10^{-12}$ m/s; and the maximum deviation of the free-surface elevation from the rest state is $\approx 1.3 \times 10^{-11}$ meters.

The fact that the free surface is essentially level suggests that the pressure forcing should be essentially zero everywhere. However, the spatial domain includes intervals where the bottom topography is variable. If the algorithm for computing the pressure forcing is not well-balanced in the presence of variable bottom topography, then in the present situation the algorithm could produce nonzero values of the pressure forcing. The wind forcing and bottom friction are zero, so the spurious pressure forcing would then yield a nonzero fluid flow. However, the fluid velocity is essentially zero everywhere, so the pressure forcing must be well-balanced in this example. This conclusion illustrates the analysis of well-balancing given in Sections 5 and 6.4.

7.1.2. Dynamic test

Next consider a test that begins with a transient phase in which the fluid flows across variable and discontinuous bottom topography. As time evolves, the system approaches a steady state that illustrates well-balanced forcing in a context that differs from that of the previous test. A motivation for a time-dependent test of well-balancing is described at the end of this subsection.

At the initial time $t = 0$, the system is at rest. Beginning at that time, a steady wind stress $\tau_{wind} = 0.1$ N/m^2 is applied in the positive y-direction on the subinterval for which 200 km $\leq x \leq$ 300 km; the x-component of wind stress is set to zero everywhere. The y-component of the wind stress generates positive values of the y-component v of velocity on the subinterval $[200, 300]$, where that stress is positive. On that subinterval, the Coriolis term $-fv$ in the x-component of the momentum equation (7) then leads to positive values of the x-component u of velocity, so the fluid begins to shift in the positive x-direction, in addition to moving down the channel. The rightward shift on the interval $[200, 300]$ causes the free surface at the top of the fluid to drop on the interval $[0, 200]$ and to rise on the interval $[300, 500]$.

The evolution of the system over time is illustrated in the bottom two frames of Fig. 4. By model day 50, the system has reached an approximate steady state, for which the velocity-dependent frictional stress at the bottom of fluid balances the wind stress at the top of the fluid, over the entire subinterval $[200, 300]$ on which the wind stress is applied. In a state of exact balance, $\rho c_D v^2 = \tau_{wind}$, which for the present choice of parameters implies $v \dot{=} 0.180$ m/s. The computed values of v on $[200, 300]$ at model day 50 are approximately 0.177 m/s, whereas the corresponding values at day 100 are approximately 0.180 m/s.

Elsewhere, the computed values of v at day 50 are approximately 10^{-3} m/s, and the computed values of u are approximately 10^{-6} m/s everywhere. The values of v at day 50 are plotted in Fig. 5.
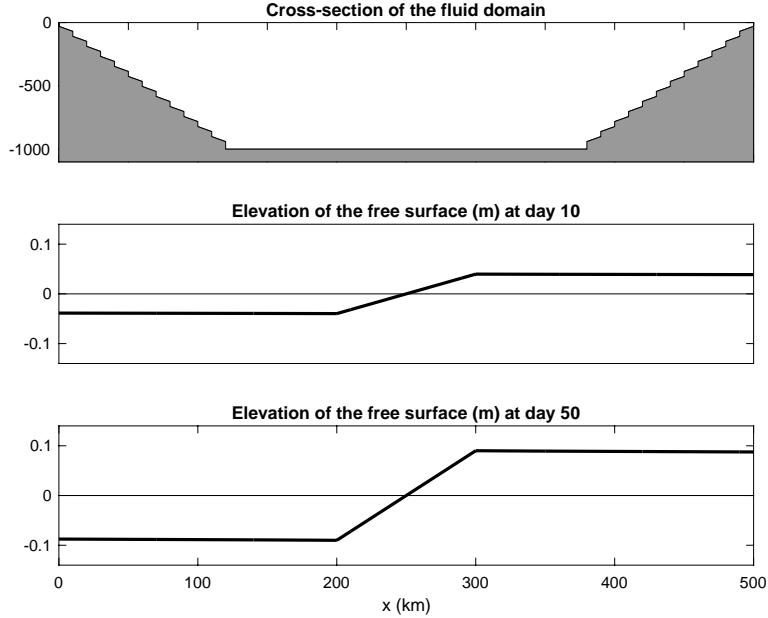
Fig. 4. A test of well-balanced forcing. The top frame shows a cross-section of an infinite straight channel; the shaded region indicates bottom topography. Vertical coordinate zero corresponds to the position of the free surface at the global rest state. Beginning at time $t = 0$, a constant wind stress is applied to the top of the fluid on the interval $200 < x < 300$. The direction of the stress is into the page. Due to the Coriolis effect, the fluid shifts to the right, and as time increases the system approaches a steady state that is characterized by a balance between the wind stress at the top of the fluid and a velocity-dependent frictional stress at the bottom of the fluid. On the portion of the domain where the bottom topography varies, the free surface is level, and the applied stresses are zero. Due to the well-balanced nature of the pressure forcing used here, the fluid is at rest on this portion of the domain by day 50.

A close-up view of the elevation of the free surface at day 50 (not included here) shows that the elevations at $x = 200$ km and $x = 300$ km are approximately -0.090 m and 0.090 m, respectively, so on the interval $[200, 300]$ the free surface has slope approximately equal to 0.18×10^{-5}. In the case of a steady state, the x-component (2) of the momentum equation reduces to $-fv = -g \partial z_{top} / \partial x$, which expresses a geostrophic balance between the Coriolis effect and the pressure forcing. For the parameters used here, this relation implies $v \approx 0.177$ m/s on the interval $[200, 300]$ at day 50, which is consistent with the remarks in the preceding paragraph.

In the approximate steady state that is computed for model day 50, the system is essentially at rest on the intervals $[0, 200]$ and $[300, 500]$, where the applied wind stress is zero. On the regions of rest, the free surface is level, so the pressure forcing should be zero on those regions. However, the regions of rest include the intervals where the bottom topography varies, so if the method for computing the pressure forcing is not well-balanced, then nonzero values of the pressure forcing could be produced on those intervals. But the fluid velocity is essentially zero on the intervals with variable bottom topography, and the applied wind stress is zero on those intervals, so the computed pressure forcing must be essentially zero there. This
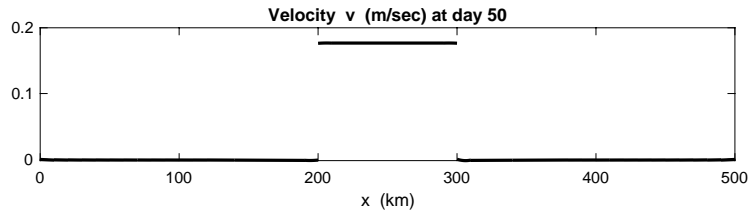
Fig. 5. The y-component v of fluid velocity at day 50. In the plots of the kind shown in Fig. 4, this velocity component is directed into the page. This component is nonzero on the portion of the spatial interval where the wind stress is applied. On that subinterval, the value of v is consistent with the slope of the free surface seen in the bottom frame of Fig. 4, in the sense that the geostrophic relation $-fv = -g\partial z_{top}/\partial x$ is satisfied on that interval.

conclusion provides another illustration of the analysis of well-balancing given in Sections 5 and 6.4.

The earlier paper [7] also contains a test of well-balancing. In that case, the system was initialized to a geostrophically-balanced state that resembles the state shown in the bottom frame of Fig. 4 in the present paper. The system remained at this state over a large number of time steps. However, the main purpose of the computations described in [7] was to examine dispersive properties of wave propagation in regions with flat bottoms, and the matter of variable bottom topography was not pursued further at that time. Subsequent work with the same code on time-dependent problems over variable bottom topography yielded some irregular behavior. This experience helped to motivate the further investigation of variable topography as described in this paper, and it motivated the introduction of a time-dependent test of well-balancing.

7.2. Propagation of a traveling wave over variable bottom topography

In this next test, the bottom elevation varies linearly over the entire spatial interval. The Coriolis parameter is $f = 0$, and the initial state is chosen so that the dynamics of the solution are nearly linear and are represented by an isolated wave pulse that propagates over the spatial interval. In this case, the wind stress and bottom stress are set to zero, so the pulse travels freely, without forcing or friction.

The analysis in the Appendix addresses the linearized shallow water equations with one horizontal dimension on a region having variable bottom topography. The analysis identifies characteristic variables w_1 and w_2, and it reduces the system to ordinary differential equations in t for w_1 and w_2 along characteristic curves $(x(t), t)$ for which $x'(t) = c(x(t)) = \sqrt{gD(x(t))}$ and $x'(t) = -c(x(t))$, respectively. Here, $D(x) > 0$ denotes the depth of the fluid at position x when the system is at the global rest state. If this depth varies with x, then the two characteristic equations are coupled, and it appears that it may be difficult to use the characteristic formulation to produce exact analytical solutions of the original system. However, the characteristic curves can be used to track the positions of the leading edge and trailing edge of a traveling and isolated pulse, and this alone can provide information about the accuracy of a numerical method.

The initial conditions are determined as follows. At time $t = 0$, the perturbation δ in the elevation of the free surface is specified to be a single cosine-squared bump centered at $\bar{x}$ with amplitude a and half-width

W. More specifically,

$$\delta(x,0) = a \left[\cos \frac{\pi}{2} \left(\frac{x - \bar{x}}{W} \right) \right]^2 \qquad \text{if } |x - \bar{x}| \leq W \tag{51}$$

and $\delta(x,0) = 0$ otherwise. The relation $p_b(x,t) = \rho g\big(D(x) + \delta(x,t)\big)$ can be used to convert this condition into a statement about the mass variable p_b that appears in the weak forms (21)–(23). In addition, the velocity u is initialized so that the characteristic variable w_2 is zero when $t = 0$; according to Eq. (A.5), this is accomplished by requiring

$$u(x,0) = \frac{c(x)\delta(x,0)}{D(x)}$$

for all x, where $c(x) = \sqrt{gD(x)}$. A comparison with Eq. (A.4) shows that the other characteristic variable w_1 satisfies $w_1(x,0) = 2c(x)\delta(x,0)$ for all x.

The right-going characteristic variable w_1 is thus initially positive on the interval $(\bar{x} - W, \bar{x} + W)$ and zero elsewhere, whereas the left-going characteristic variable w_2 is initially zero everywhere. The resulting solution thus consists primarily of a right-going wave. Coupling between w_1 and w_2, as represented in the right side of Eq. (A.8), implies that nonzero values of $w_2(x,t)$ could be generated for $t > 0$; however, the plots in Figs. 7, 8, and 10 suggest that this effect is small, in the present example.

In this test, the spatial interval is $[0, L]$, with $L = 2000$ km. The length of each grid cell is $\Delta x = 10$ km, so the spatial interval $[0, L]$ is partitioned into 200 cells of equal length. For the initial state (51) of the elevation of the free surface, the center of the cosine-squared bump is $\bar{x} = 200$ km, the amplitude is $a = 0.1$ m, and the half-width W has values that are discussed below. In the computations described here, the maximum depth of the fluid is 4000 m; for reasons analogous to those given in Section 7.1, the time increment Δt is then chosen to be 8 seconds.

For the first set of computations, the bottom topography is continuous, with the depth D varying linearly from $D(0) = 4000$ m to $D(L) = 10$ m. This is illustrated in the top frame in Fig. 6. The bottom frame shows the elevation of the free surface at the initial time, in the case where $W = 8\Delta x$, i.e., the pulse at the initial time has a width of 16 grid cells.

Fig. 7 shows the computed values of the free-surface elevation, for $W = 8\Delta x$, after 1000, 1500, and 2000 time steps. In each frame in the plot, the vertical dotted lines designate the locations of the leading edge and the trailing edge of the propagating wave in the exact solution. These locations are determined from Eq. (A.9), which gives the position at time t of the characteristic curve with positive velocity that has position x_0 at time 0. This formula is applied twice, with $x_0 = \bar{x} + 8\Delta x$ for the leading edge of the wave and $x_0 = \bar{x} - 8\Delta x$ for the trailing edge. The plots in Fig. 7 show that the location of the pulse, as propagated during the numerical computation, is essentially the same as the location in the exact analytical solution.

The plots in Fig. 7 show that the propagated pulse becomes narrower as time increases. Because of the shape of the bottom topography, the velocity $c(x) = \sqrt{gD(x)}$ is smaller at the leading edge of the wave
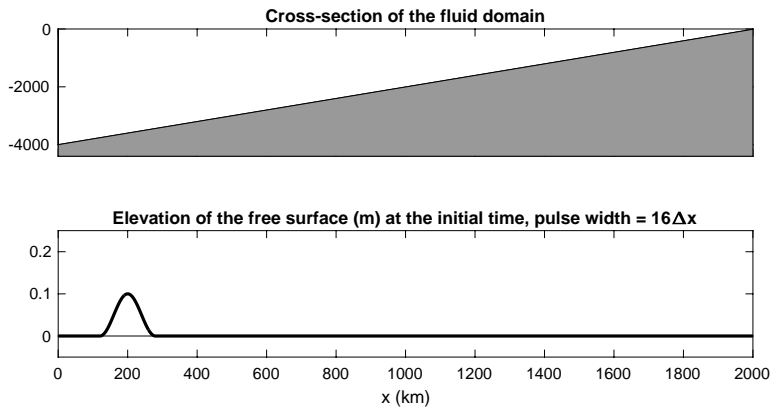
Fig. 6. Propagation of a traveling wave over variable bottom topography. The upper frame shows the bottom topography that is used for the computations illustrated in Figs. 7 and 8. In this case, the elevation of the bottom is continuous and varies linearly from -4000 m to -10 m. The lower frame shows the initial state for the solution illustrated in Fig. 7; here, the nonzero part of the curve is a cosine-squared pulse having a width of 16 grid cells. The fluid velocity is initialized so as to produce a right-going wave.

than it is at the trailing edge, so the trailing edge partially catches up to the leading edge. At time step 2000, the width of the pulse in the exact solution is only about 2.7 grid cells.

A computation with even lower resolution is illustrated in Fig. 8. In that case, the width of the pulse at the initial time is 4 grid cells, and at time step 2000 the width of the pulse in the exact solution is less than one grid cell. By conventional standards, the pulse is highly under-resolved, and with this kind of resolution it would not be possible to obtain an accurate representation of the shape of the pulse. However, in spite of the lack of resolution, the energy in the wave is nonetheless found in the correct location. Some further comments on this point are given below, in Section 7.3.

The final computation tests the ability of the DG method to handle discontinuities in bottom topography at the edges of grid cells. The formulation of the problem is the same as for the solution shown in Fig. 7, except that the topography is constant in each grid cell, so as to produce a stairstep pattern. A portion of the bottom of the fluid is illustrated in Fig. 9. The computed solution is shown in Fig. 10. The results are very similar to those shown in Fig. 7, so in this case the presence of discontinuities has little effect on the computed solution.

7.3. Remarks on grid resolution

Above, it was pointed out that the DG algorithm causes the propagated energy in the computed wave to be at the correct location, even if the wave shape itself is not well-resolved. An analogue of this result was found in the analysis and computations reported in [7] for the case of linear inertia-gravity waves in one horizontal dimension with level bottom topography. Dispersion relations for such waves, for the case of the DG methods described in [7], agree very closely with the dispersion relations for exact solutions. This statement applies to all wavenumbers that could be seen in a numerical solution, not just those wavenumbers corresponding to at least several grid intervals per wavelength. This property is not typically
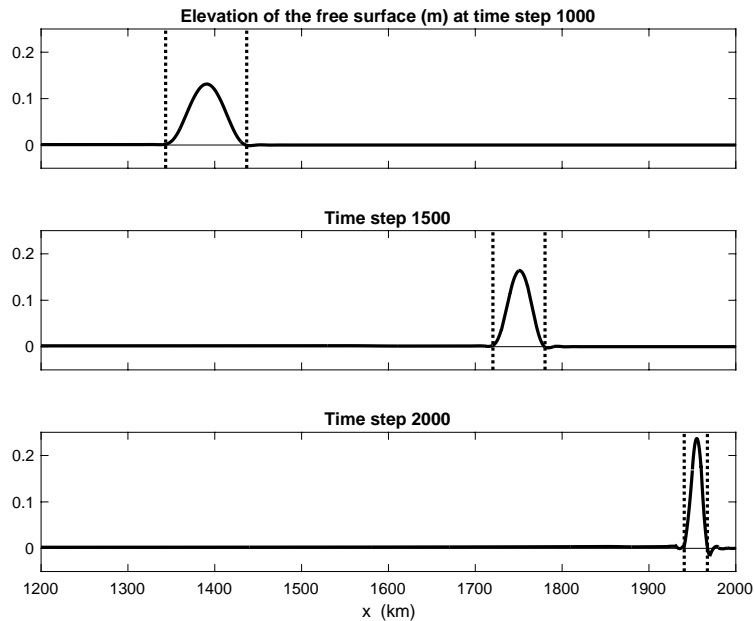
Fig. 7. Computed values of the free-surface elevation for the case where the pulse initially has width $16\Delta x$. In each plot, the vertical dotted lines indicate the locations of the leading and trailing edges of the pulse in the exact solution. For the sake of visibility, the solution is plotted on the subinterval 1200 km $\leq x \leq 2000$ km instead of the entire interval $0 \leq x \leq 2000$. Due to the varying depth of the fluid, the front edge of the pulse always travels more slowly than the trailing edge of the pulse, so the pulse becomes narrower as it propagates. At time step 1000, the pulse in the exact solution has width approximately equal to 9.4 grid cells; at step 1500, the width is approximately 6.0 cells; at step 2000, the width is approximately 2.7 cells. Despite the low resolution near the end of the time interval, the energy in the computed solution is at the correct location.

found in finite difference methods, and some standard finite difference methods are included in the analysis and computations in [7]. The result for DG methods suggests that correct group and phase velocities can be found in computed solutions, even for modes that are not well-resolved in a conventional sense. The analysis is supported by some numerical experiments involving the propagation of wave packets; in the experiments reported in [7], the energy was always in the correct location in the case of a DG method, even if the wave was not well-resolved, whereas this was not always the case with finite difference methods.

One way to assess the accuracy of a numerical method is to test rates of convergence as $\Delta x \to 0$ and $\Delta t \to 0$. The preceding remarks refer to the opposite extreme of examining behavior at the limits of low resolution. Geophysical fluid flows typically exhibit broad ranges of length and time scales, and the preceding results suggest a potential advantage of discontinuous Galerkin methods for this application.

8. Summary

A central idea in this paper is to use integral weak forms for the shallow water equations that lead to discontinuous Galerkin numerical methods that are naturally adapted to variable bottom topography. This is one step towards implementing variable topography in DG methods for multi-layer models, as the fast equations in a barotropic-baroclinic time splitting for a multi-layer model are very similar to the constant-
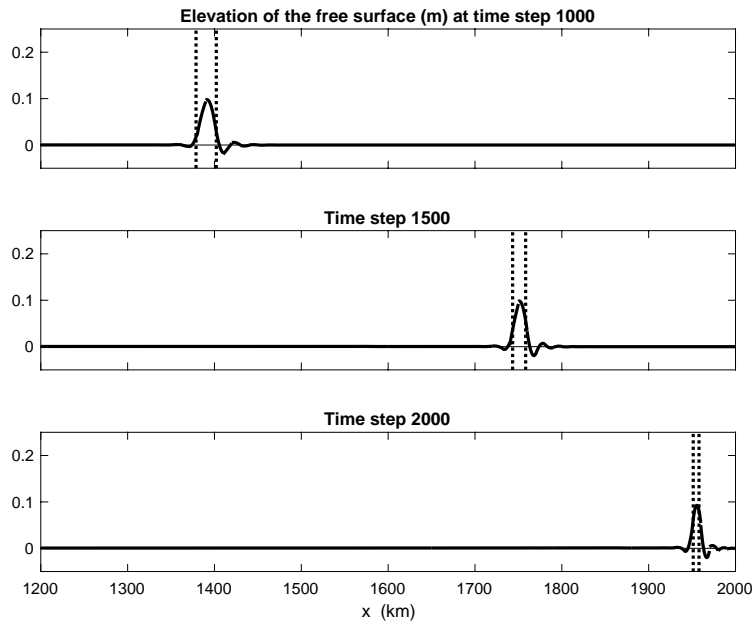
Fig. 8. Solution at a very low resolution. At the initial time, the pulse has width $4\Delta x$. **At time step** 1000, **the pulse in the exact solution has width approximately equal to** 2.3 **grid cells; at step** 1500, **the width is approximately** 1.5 **cells; at step** 2000, **the width is approximately** 0.7 **cells.**
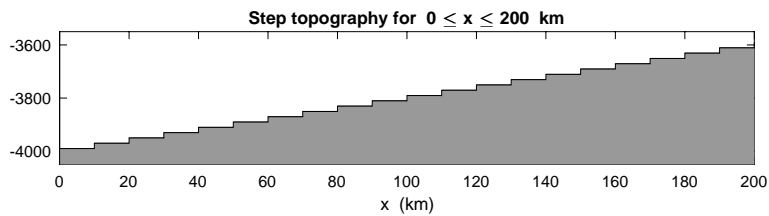
Fig. 9. Bottom topography for the solution illustrated in Fig. 10. In this case, the elevation of the bottom is constant in each grid cell, with the midpoints of the topography in each cell lying on the same line that is plotted in Fig. 6 for the case of continuous topography. For the sake of visibility, this plot shows the subinterval $0 \leq x \leq 200$ **instead of the entire interval** $0 \leq x \leq 2000$. **At each cell edge, the vertical jump is approximately** 20 **m.**

density shallow water equations for a single layer.

A crucial step in this development is the representation of the pressure forcing in the momentum equations. Instead of working with pointwise partial differential equations involving velocity and layer thickness, the approach taken here is to start with the basic form $\partial P/\partial x$ of the pressure forcing and then proceed directly to a weak form by multiplying by a test function, integrating over the water column that resides in a grid cell, and applying a multi-dimensional integration by parts. A numerical implementation of the resulting formula requires the computation of certain quantities at the edges of grid cells, based on the values in the adjacent grid cells. This paper uses a Riemann problem at cell edges to develop one such method for doing this interpolation. More generally, it is assumed here that any method for performing this task must reproduce the continuous values in the case where all of the functions involved are continuous.
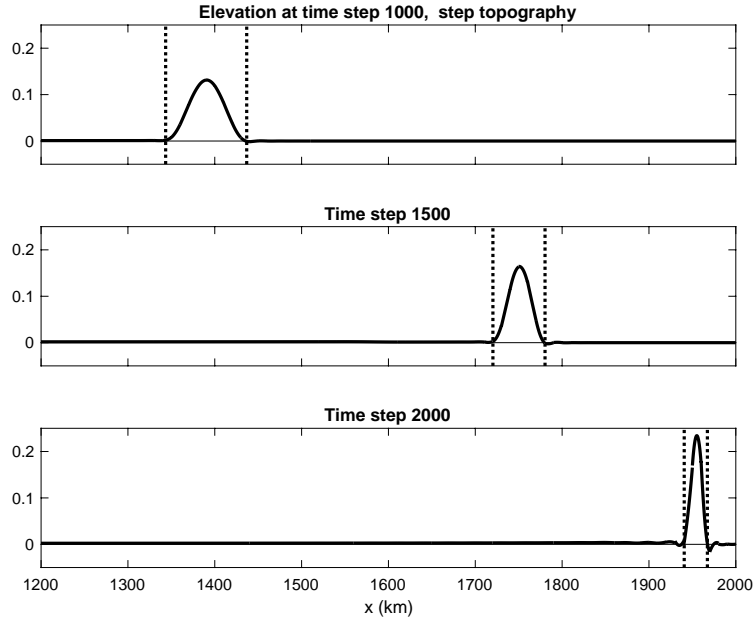
Fig. 10. Computed solution for the case where the bottom topography is piecewise constant. At the initial time, the pulse has width $16\Delta x$, which is also the case for the solution plotted in Fig. 7 for the case of continuous topography. The computed solutions for the two cases are very similar; slight differences can be seen at the trailing edge of the pulse at time step 2000.

Subject to this assumption, the representation of pressure forcing that is developed here is well-balanced. The main idea behind the well-balancing is the following. If the free surface is level on a grid cell, then one wants the computed value of the pressure forcing to be zero. In the case of a level free surface, $\partial P/\partial x = 0$ on the region of integration, so the integral mentioned in the preceding paragraph is zero. But the representation of the pressure forcing is a result of manipulating that integral, so one expects that the implemented formula for the pressure forcing should therefore be zero. However, in this analysis it is necessary to be careful at the edges of the grid cell, and that is the reason for the assumption regarding continuity for the interpolation method at the cell edges.

This formulation produces good results in some numerical computations involving a stationary well-balanced problem, a time-dependent problem that leads to a well-balanced steady state, and another problem that involves the propagation of a traveling wave on a region with variable bottom topography. In the latter case, the energy in the computed wave is in the correct location, even in low-resolution simulations where the grid is too coarse to provide good resolution of the shape of the wave form itself.

Appendix A. A test problem

This Appendix develops a test problem involving the propagation of traveling waves in a region with variable bottom topography.

As in Section 6.1, consider a linearized system with Coriolis parameter zero. However, in the present case do not assume that the bottom elevation z_{bot} is constant, and instead let $D(x) > 0$ denote the depth of the

fluid at position x when the fluid is at the global rest state. As before, let $\delta(x,t)$ denote the perturbation in the elevation of the free surface from that state. In this case, the analogue of the system in Eqs. (35)–(36) is

$$\frac{\partial u}{\partial t} = -g\frac{\partial \delta}{\partial x}$$

$$\frac{\partial \delta}{\partial t} + \frac{\partial}{\partial x}\Big(D(x)u\Big) = 0.$$

For the following analysis, some simplifications can be made by letting $q(x,t) = D(x)u(x,t)$ for all (x,t); the quantity $q(x,t)$ is a constant multiple of momentum density and of mass flux. The preceding system then becomes

$$\frac{\partial q}{\partial t} + gD(x)\frac{\partial \delta}{\partial x} = 0$$

$$\frac{\partial \delta}{\partial t} + \frac{\partial q}{\partial x} = 0;$$

in matrix-vector form, this system is

$$\frac{\partial}{\partial t}\begin{pmatrix} q \\ \delta \end{pmatrix} + \begin{pmatrix} 0 & c(x)^2 \\ 1 & 0 \end{pmatrix}\frac{\partial}{\partial x}\begin{pmatrix} q \\ \delta \end{pmatrix} = \begin{pmatrix} 0 \\ 0 \end{pmatrix}, \tag{A.1}$$

where $c(x) = \sqrt{gD(x)}$. Solutions of the system (A.1) will be analyzed here with an analogue of the idea of Riemann invariants (LeVeque [10]).

In the case where D is constant, the simple analysis in Section 6.1 shows that signals propagate with the constant velocities $\pm c$, where $c = \sqrt{gD}$. However, if c is not constant then the analysis in Section 6.1 does not apply. The analysis in this Appendix generalizes the earlier analysis to the case where c varies with location.

Appendix A.1. Derivation of characteristic equations

Let $A(x)$ denote the 2×2 matrix on the left side of Eq. (A.1). For each x, the eigenvalues of $A(x)$ are $\lambda_1(x) = c(x)$ and $\lambda_2(x) = -c(x)$. Corresponding left eigenvectors are $\ell_1(x) = \big(1, \ c(x)\big)$ and $\ell_2(x) = \big(1, \ -c(x)\big)$, respectively; that is, $\ell_1(x)A(x) = \lambda_1(x)\ell_1(x)$ and $\ell_2(x)A(x) = \lambda_2(x)\ell_2(x)$. The following calculations require functions $\phi_1(q,\delta,x)$ and $\phi_2(q,\delta,x)$ for which

$$\nabla\phi_1(q,\delta,x) = \left(\frac{\partial\phi_1}{\partial q}, \frac{\partial\phi_1}{\partial\delta}\right) = \ell_1(x) = \big(1, \ c(x)\big)$$

$$\nabla\phi_2(q,\delta,x) = \left(\frac{\partial\phi_2}{\partial q}, \frac{\partial\phi_2}{\partial\delta}\right) = \ell_2(x) = \big(1, \ -c(x)\big);$$

Here, the symbols q and δ refer to independent variables, not functions of (x,t), and the gradient notation ∇ refers to partial derivatives with respect to q and δ but not x. For the present purposes, let

$$\phi_1(q,\delta,x) = q + c(x)\delta \tag{A.2}$$

$$\phi_2(q,\delta,x) = q - c(x)\delta.$$

Pre-multiply the system (A.1) by the row vector $\ell_1(x) = (\partial\phi_1/\partial q, \partial\phi_1/\partial\delta)$ and use the relation $\ell_1 A = \lambda_1\ell_1 = c\ell_1$ to obtain

$$\frac{\partial\phi_1}{\partial q}q_t \;+\; \frac{\partial\phi_1}{\partial\delta}\delta_t \;+\; c(x)\left(\frac{\partial\phi_1}{\partial q}q_x \;+\; \frac{\partial\phi_1}{\partial\delta}\delta_x\right) \;=\; 0.$$

It then follows that

$$\frac{\partial}{\partial t}\Big[\phi_1\big(q(x,t),\delta(x,t),x\big)\Big] \;+\; c(x)\frac{\partial}{\partial x}\Big[\phi_1\big(q(x,t),\delta(x,t),x\big)\Big] \;=\; c(x)\frac{\partial\phi_1}{\partial x}\big(q(x,t),\delta(x,t),x\big). \qquad \text{(A.3)}$$

The partial derivatives on the left side of this equation are derivatives of composite functions, whereas the derivative on the right side is $\partial\phi_1/\partial x$ evaluated at $\big(q(x,t),\delta(x,t),x\big)$. A comparison with Eq. (A.2) shows $\partial\phi_1/\partial x = c'(x)\delta$; recall that in (A.2), q and δ are independent variables, not functions of (x,t). The right side of Eq. (A.3) is then $c(x)c'(x)\delta(x,t)$. But $c(x) = \sqrt{gD(x)}$, and a calculation shows that the right side of Eq. (A.3) is $\frac{g}{2}D'(x)\delta(x,t)$.

Now let

$$w_1(x,t) \;=\; \phi_1\big(q(x,t),\delta(x,t),x\big)$$
$$=\; q(x,t) + c(x)\delta(x,t) \;=\; D(x)u(x,t) + c(x)\delta(x,t) \qquad\qquad\qquad \text{(A.4)}$$

$$w_2(x,t) \;=\; \phi_2\big(q(x,t),\delta(x,t),x\big)$$
$$=\; q(x,t) - c(x)\delta(x,t) \;=\; D(x)u(x,t) - c(x)\delta(x,t). \qquad\qquad\qquad \text{(A.5)}$$

The right side of Eq. (A.3) can then be expressed as

$$\frac{g}{2}D'(x)\delta(x,t) \;=\; \frac{g}{4c(x)}D'(x)\Big[w_1(x.t) - w_2(x,t)\Big]. \qquad\qquad\qquad \text{(A.6)}$$

A comparison of Eqs. (A.3) and (A.6) shows

$$\frac{\partial w_1}{\partial t} \;+\; c(x)\frac{\partial w_1}{\partial x} \;=\; \frac{g}{4c(x)}D'(x)\Big[w_1(x.t) - w_2(x,t)\Big], \qquad\qquad\qquad \text{(A.7)}$$

and a similar analysis of ϕ_2 and w_2 shows

$$\frac{\partial w_2}{\partial t} \;-\; c(x)\frac{\partial w_2}{\partial x} \;=\; \frac{g}{4c(x)}D'(x)\Big[w_1(x.t) - w_2(x,t)\Big]. \qquad\qquad\qquad \text{(A.8)}$$

The left side of Eq. (A.7) represents a derivative of w_1 along characteristic curves having velocity $c(x)$. More precisely, consider any characteristic curve $(x(t),t)$ for which $x'(t) = c(x(t))$ for all $t > 0$. Then Eq. (A.7) implies

$$\frac{d}{dt}\big(w_1\big(x(t),t\big)\big) \;=\; \frac{g}{4c\big(x(t)\big)}D'\big(x(t)\big)\Big[w_1\big(x(t),t\big) - w_2\big(x(t),t\big)\Big]$$

for all t. Similarly, the left side of Eq. (A.8) represents a derivative of w_2 along characteristic curves having velocity $-c(x)$.

If the bottom elevation z_{bot} is constant, then $D'(x) = 0$ for all x, and Eqs. (A.7) and (A.8) for w_1 and w_2 are uncoupled. It is then straightforward to use initial data to find exact solutions of the system

(A.1). On the other hand, if D' is nonzero, then the system (A.7)–(A.8) is coupled and thus is considerably more complicated. However, it is still possible to use the flow along characteristics to track the leading and trailing edges of traveling waves, and this is done during the description of numerical computations in Section 7.2.

Appendix A.2. The case of linearly-varying bottom topography

The analysis in the preceding subsection describes a sense in which signals propagate with characteristic velocities $\pm c(x)$, where $c(x) = \sqrt{gD(x)}$. The present subsection develops explicit formulas for the case where D varies linearly with x, i.e., the bottom elevation z_{bot} varies linearly with x.

Assume that the shallow water equations are posed on the spatial interval $[0, L]$, with solid-wall boundary conditions imposed at the endpoints of this interval. Also assume that D varies linearly on that interval, and for the sake of definiteness assume $D(0) > D(L)$. For notational convenience, express $D(x)$ in the form

$$D(x) = D(0) \left(1 - \frac{x}{M}\right)$$

for $0 \le x \le L$; if $D(x)$ were extended linearly for $x > L$, then $x = M$ would be the point where $D(x)$ reaches 0. It follows that $M = D(0)L/\big(D(0) - D(L)\big)$.

Consider any characteristic curve $(x(t), t)$ for which $x'(t) = c(x(t))$ for $t > 0$. In this case,

$$x'(t) \;=\; \sqrt{gD(x(t))} \;=\; \sqrt{gD(0)\left(1 - \frac{x(t)}{M}\right)} \;=\; c_0\sqrt{1 - \frac{x(t)}{M}},$$

where $c_0 = \sqrt{gD(0)}$ denotes the value of c when $x = 0$. An integration and some algebraic manipulations yield

$$x(t) \;=\; M - \frac{c_0^2}{4M}(t - K)^2,$$

where K is a constant. Now consider the characteristic curve of this form that passes through any point $(x_0, 0)$ for which $0 < x_0 < L$, i.e., for which $x(0) = x_0$. Some further manipulations yield that, for this characteristic curve,

$$x(t) \;=\; M - \frac{c_0^2}{4M} \left[t - \frac{2}{c_0}\sqrt{M(M - x_0)}\right]^2 \tag{A.9}$$

for all $t \ge 0$ for which $x(t)$ lies in the interval $[0, L]$.

Next consider the characteristic curve $(x(t), t)$ that passes through $(x_0, 0)$ and has the negative velocity $x'(t) = -c(x(t)) = -\sqrt{gD(x(t))}$ for $t > 0$. A similar calculation shows

$$x(t) \;=\; M - \frac{c_0^2}{4M} \left[t + \frac{2}{c_0}\sqrt{M(M - x_0)}\right]^2 . \tag{A.10}$$

The formulas in Eqs. (A.9) and (A.10) can then be used to track the positions of traveling waves, as is done in Section 7.2.

References

[1] A. Adcroft, R. Hallberg, M. Harrison, A finite volume discretization of the pressure gradient force using analytic integra-
     tion, Ocean Modelling 22 (2008) 106–113.
[2] R. Bleck, L.T. Smith, A wind-driven isopycnic coordinate model of the north and equatorial Atlantic Ocean 1. Model
     development and supporting experiments, J. Geophysical Research 95C (1990) 3273–3285.
[3] B. Bonev, J.S. Hesthaven, F.X. Giraldo, M.A. Kopera, Discontinuous Galerkin scheme for the spherical shallow water
     equations with applications to tsunami modeling and prediction, J. Comput. Phys. 362 (2018) 425–448.
[4] C. Dawson, E.J. Kubatko, J.J. Westerink, C. Trahan, C. Mirabito, C. Michoski, N. Panda, Discontinuous Galerkin
     methods for modeling hurricane storm surge, Advances in Water Resources 34 (2011) 1165–1176.
[5] A.E. Gill, Atmosphere-Ocean Dynamics, Academic Press, San Diego, 1982.
[6] R.L. Higdon, Numerical modelling of ocean circulation, Acta Numerica 15 (2006) 385–470.
[7] R.L. Higdon, Pressure forcing and dispersion analysis for discontinuous Galerkin approximations to oceanic fluid flows, J.
     Comput. Phys. 249 (2013) 36–66.
[8] R.L. Higdon, Multiple time scales and pressure forcing in discontinuous Galerkin approximations to layered ocean models,
     J. Comput. Phys. 295 (2015) 230–260.
[9] R.L. Higdon, Discontinuous Galerkin methods for multi-layer ocean modeling: Viscosity and thin layers, J. Comput. Phys.
     401 (2020) 109018.
[10] R.J. LeVeque, Finite Volume Methods for Hyperbolic Problems, Cambridge University Press, Cambridge, UK, 2002.
[11] R.J. LeVeque, D.L. George, M.J. Berger, Tsunami modelling with adaptively refined finite volume methods, Acta Numerica
     20 (2011) 211–289.
[12] S.J. Lin, A finite-volume integration method for computing pressure gradient force in general vertical coordinates, Q. J.
     R. Meteorol. Soc. 123 (1997) 1749–1762.
[13] X. Liu, A well-balanced and positivity-preserving numerical model for shallow water flows in channels with wet–dry fronts,
     J. Sci. Comput. 85 (2020) 60–81.
[14] W.J. Pringle, D. Wirasaet, A. Suhardjo, J. Meixner, J.J. Westerink, A.B. Kennedy, S. Nong, Finite-element barotropic
     model for the Indian and western Pacific Oceans: Tidal model-data comparisons and sensitivities, Ocean Modelling 129
     (2018) 13–38.
[15] G.K. Vallis, Atmospheric and Oceanic Fluid Dynamics: Fundamentals and Large-Scale Circulation, Cambridge University
     Press, Cambridge, UK, 2nd edition, 2017.
[16] Y. Xing, X. Zhang, C.W. Shu, Positivity-preserving high order well-balanced discontinuous Galerkin methods for the
     shallow water equations, Advances in Water Resources 33 (2010) 1476–1493.
[17] R. Yang, Y. Yang, Y. Xing, High order sign-preserving and well-balanced exponential Runge-Kutta discontinuous Galerkin
     methods for the shallow water equations with friction, J. Comput. Phys. (2021) 110543.